γ-ray spectroscopy of $^{16}_{\Lambda}$O and $^{15}_{\Lambda}$N hypernuclei via the ^{16}O($K^-, \pi^-\gamma$) reaction

M. Ukai,[1,*] S. Ajimura,[2] H. Akikawa,[3,†] D. E. Alburger,[4] A. Banu,[5] R. E. Chrien,[4] G. B. Franklin,[6] J. Franz,[7] O. Hashimoto,[1]
T. Hayakawa,[2] H. Hotchi,[4,‡] K. Imai,[3] T. Kishimoto,[2] M. May,[4] D. J. Millener,[4] S. Minami,[2,§] Y. Miura,[1] T. Miyoshi,[1,∥]
K. Mizunuma,[1] T. Nagae,[8,¶] S. N. Nakamura,[1] K. Nakazawa,[9] Y. Okayasu,[1] P. Pile,[4] B. P. Quinn,[6] A. Rusek,[4] Y. Sato,[8]
R. Sutter,[4] H. Takahashi,[3,**] L. Tang,[10] H. Tamura,[1] K. Tanida,[11,¶] and S. H. Zhou[12]

(E930('01) Collaboration)

[1]*Department of Physics, Tohoku University, Sendai 980-8578, Japan*
[2]*Department of Physics, Osaka University, Toyonaka 560-0043, Japan*
[3]*Department of Physics, Kyoto University, Kyoto 606-8502, Japan*
[4]*Brookhaven National Laboratory, New York 11973, USA*
[5]*GSI, Darmstadt D-64291, Germany*
[6]*Carnegie Mellon University, Pittsburgh, Pennsylvania 15213, USA*
[7]*Department of Physics, University of Freiburg, Freiburg D-79104, Germany*
[8]*Institute of Particle and Nuclear Studies, KEK, Tsukuba 305-0801, Japan*
[9]*Department of Physics, Gifu University, Gifu 501-1193, Japan*
[10]*Department of Physics, Hampton University, Hampton, Virginia 23668, USA*
[11]*RIKEN, Wako 351-0198, Japan*
[12]*Department of Physics, China Institute of Atomic Energy, P. O. Box 275(80), Beijing 102413, People's Republic of China*

The bound-state level structures of the $^{16}_{\Lambda}$O and $^{15}_{\Lambda}$N hypernuclei were studied by γ-ray spectroscopy using a germanium detector array (Hyperball) via the ^{16}O ($K^-, \pi^-\gamma$) reaction. A level scheme for $^{16}_{\Lambda}$O was determined from the observation of three γ-ray transitions from the doublet of states ($2^-, 1^-$) at $\sim$6.7 MeV to the ground-state doublet ($1^-, 0^-$). The $^{15}_{\Lambda}$N hypernuclei were produced via proton emission from unbound states in $^{16}_{\Lambda}$O. Three γ rays were observed, and the lifetime of the $1/2^+$; 1 state in $^{15}_{\Lambda}$N was measured by the Doppler shift attenuation method. By comparing the experimental results with shell-model calculations, the spin dependence of the ΛN interaction is discussed. In particular, the measured $^{16}_{\Lambda}$O ground-state doublet spacing of $26.4 \pm 1.6 \pm 0.5$ keV determines a small but nonzero strength of the ΛN tensor interaction.

I. INTRODUCTION

We have performed a series of experiments on the γ-ray spectroscopy of Λ hypernuclei using a germanium detector array called Hyperball [1–3]. The main purpose of these experiments is to study the spin dependence of the ΛN interaction via precise measurements of level spacings in p-shell hypernuclei. In this paper, we report on results for the $^{16}_{\Lambda}$O and $^{15}_{\Lambda}$N hypernuclei investigated via the ^{16}O(K^-, π^-) reaction at the Brookhaven National Laboratory.

---

*Present address: Department of Physics, Gifu University, Gifu 501-1193, Japan.

†Present address: Accelerator Laboratory, KEK, Tsukuba 305-0801, Japan.

‡Present address: Japan Atomic Energy Agency, Tokai 319-1195, Japan.

§Present address: GSI, Darmstadt D-64291, Germany.

∥Present address: Institute of Materials Structure Science, KEK, Tsukuba 305-0801, Japan.

¶Present address: Department of Physics, Kyoto University, Kyoto 606-8502, Japan.

**Present address: Institute of Particle and Nuclear Studies, KEK, Tsukuba 305-0801, Japan.

A. ΛN spin-dependent interactions

In principle, interactions between baryons can be studied by baryon-baryon scattering experiments. However, such scattering experiments are extremely difficult except for the nucleon-nucleon (NN) case due to the short lifetimes of the other baryons. On the other hand, Λ-hypernuclear data can provide information on the ΛN interaction.

Free hyperon-nucleon (YN) interaction models have been theoretically constructed as extensions of NN interaction models by assuming flavor SU(3) symmetry [4,5]. Effective YN interactions have often been approximated as a G matrix derived from the free YN interaction, either in nuclear matter as a function of density [6] or using the Pauli exclusion operator for finite nuclei [7]. Many-body effects entering into the calculation of the effective interaction for a finite shell-model space from the G matrix are small, except for the effects of coupling Λ-hypernuclear and Σ-hypernuclear states (Λ-Σ coupling) [8]. This is in part due to the lack of Pauli blocking for a Λ in a Λ hypernucleus and in part because the ΛN interaction is relatively weak because one-pion exchange is forbidden due to isospin conservation. On the other hand, the ΛN-ΣN interaction can be mediated by one-pion exchange, and it is found to play a significant role in the energy-level spacings of s-shell hypernuclei despite the $\sim$80 MeV Λ-Σ mass difference [9–12].

A hypernucleus ($_\Lambda^A$Z) has a spin-doublet ($J \pm 1/2$) structure when the core nuclear ($^{A-1}$Z) level has nonzero spin ($J \neq 0$) and the Λ is in the $0s$ orbit. In this simple weak-coupling limit, the splitting of the doublet is due only to ΛN interactions that involve the Λ spin [see Eq. (1) below] together with a contribution from Λ-Σ coupling. Therefore, such spin-doublet structures in hypernuclei provide us with information on the spin dependence of the ΛN interaction.

The ΛN effective interaction [13,14] can be written in the form

$$
\begin{aligned}
V_{\Lambda N} = {} & V_0(r) + V_\sigma(r)\, \boldsymbol{s}_N \cdot \boldsymbol{s}_\Lambda \\
& + V_\Lambda(r)\, \boldsymbol{l}_{N\Lambda} \cdot \boldsymbol{s}_\Lambda + V_N(r)\, \boldsymbol{l}_{N\Lambda} \cdot \boldsymbol{s}_N \\
& + V_T(r)\, [3(\boldsymbol{\sigma}_N \cdot \hat{\boldsymbol{r}})(\boldsymbol{\sigma}_\Lambda \cdot \hat{\boldsymbol{r}}) - \boldsymbol{\sigma}_N \cdot \boldsymbol{\sigma}_\Lambda].
\end{aligned} \quad (1)
$$

The terms correspond to the spin-averaged and spin-spin central, the Λ-spin-dependent spin-orbit (Λ-spin-orbit), the nucleon-spin-dependent spin-orbit (N-spin-orbit), and the tensor interactions, respectively. For s_Λ configurations in p-shell hypernuclei, there are five independent two-body matrix elements $\langle p_N s_\Lambda | V_{\Lambda N} | p_N s_\Lambda \rangle$ that can be written in terms of radial integrals associated with each of these terms. The radial integrals are conventionally denoted by the parameters $\overline{V}$, Δ, S_Λ, S_N, and T, respectively [13,14], with S_Λ and S_N the coefficients of $\boldsymbol{l}_N \cdot \boldsymbol{s}_\Lambda$ and $\boldsymbol{l}_N \cdot \boldsymbol{s}_N$ (because $\boldsymbol{l}_{N\Lambda}$ is proportional to $\boldsymbol{l}_N$ for a Λ in an s orbit). Since $\overline{V}$ contributes equally to all levels, the level spacings are given by a linear combination of the four spin-dependent parameters and corresponding core level spacings. As noted above, only Δ, S_Λ, and T contribute to doublet spacings in the weak-coupling limit.

For the same p-shell model space, the ΛN-ΣN interaction can be written and parametrized in the same way as the ΛN effective interaction [15]. For a fixed Λ-Σ coupling interaction, the four ΛN parameters that govern the spin dependence of the interaction can be determined phenomenologically to fit various p-shell hypernuclear level spacings. In particular, a level spacing that is dominantly given by one parameter provides the parameter value almost independently of the others. For example, if the core state has $L = 0$, only Δ contributes to the doublet spacing. This is the case for the ground-state doublet spacing in $_\Lambda^7$Li ($3/2^+$, $1/2^+$) due to an almost pure $^3S_1$ configuration for the core ^{6}Li(1^+). Similarly, if the ^{8}Be(2^+) core state for the excited-state doublet in $_\Lambda^9$Be ($3/2^+$, $5/2^+$) has $L = 2$ and $S = 0$, only S_Λ contributes to the doublet spacing. Then, by comparing the experimentally determined parameter values with the predicted values by theoretical models of YN interactions, we can test the validity of the models.

However, effects of YN interactions on hypernuclear levels are small. In particular, spin-doublet spacings of p-shell and heavier hypernuclei are expected to be much smaller than 1 MeV. In some cases, hypernuclei have quite small spin-doublet spacings of the order of a few tens of keV, leading to the use of the term "hypernuclear fine structure." Therefore, an energy resolution of the order of several keV is necessary for spectroscopic studies to resolve the level spacings. Thus, γ-ray spectroscopy with germanium (Ge) detectors has exclusive access to these structures.

For this purpose, a Ge detector array dedicated to the γ-ray spectroscopy of hypernuclei, Hyperball, was built in 1998 [16], and a project was started to investigate the precise structure of hypernuclei.

B. Previous studies

The energy levels of Λ hypernuclei were studied by (K^-, π^-) and (π^+, K^+) reaction spectroscopy and by γ-ray spectroscopy with NaI counters prior to the start of the Hyperball project in 1998.

Information on the spin-spin interaction can be obtained from the observations of the ~ 1.1 MeV spin-flip $M1$ transitions between the ground-state doublet ($1^+ \to 0^+$) in $_\Lambda^4$H and $_\Lambda^4$He with NaI counters [17]. However, it has been shown that Λ-Σ coupling can make a large contribution to these doublet spacings [18]. Recently, four-body calculations have been performed [9–12] for a number of the Nijmegen YN potential models with the result that both the spin-spin interaction and Λ-Σ coupling make significant (comparable) contributions to the splitting.

A small Λ-spin-orbit interaction was reported for the first time based on the fact that the splitting between the $p_{1/2}$ and $p_{3/2}$ substitutional states in $_\Lambda^{16}$O is close to that of the underlying hole states of the ^{15}O core [19,20]. Afterward, the γ-ray spectroscopy of $_\Lambda^9$Be with NaI counters suggested a very small spin-orbit strength corresponding to $|S_\Lambda| < 0.04$ MeV from a limit of < 100 keV for the spacing of the 3-MeV excited-state doublet ($3/2^+$, $5/2^+$) based on the fact that the width of the peak containing both γ rays was comparable with the resolution of ~ 160 keV [21].

In 1998, high-precision γ-ray spectroscopy experiments for $_\Lambda^7$Li and $_\Lambda^9$Be were carried out with Hyperball using the ^{7}Li(π^+, $K^+\gamma$) and the ^{9}Be (K^-, $\pi^-\gamma$) reactions, respectively [1,2]. The ground-state doublet spacing of 692 keV in $_\Lambda^7$Li provided a spin-spin parameter value of $\Delta \sim 0.5$ MeV without the inclusion of Λ-Σ coupling. In the p shell, the scale of energy shifts due to Λ-Σ coupling is expected to be roughly a factor of 4 smaller (with a strong state dependence) than that for the $A = 4$ hypernuclei [15], and provides only about 12% of the ground-state doublet spacing in $_\Lambda^7$Li. A strength of $S_N \sim -0.4$ MeV was also established from the excitation energy of the $5/2^+$ state in $_\Lambda^7$Li [1].

In the next experiment, the rather small spacing of the $3/2^+$, $5/2^+$ doublet in $_\Lambda^9$Be noted above was resolved [2]. The $3/2^+$ state has been determined to be the upper member of the doublet based on ^{10}B target data from the present experiment [3,15]. The spacing of 43(5) keV leads to $-0.02 < S_\Lambda < -0.01$ MeV [3]. The sign and magnitude of S_Λ are consistent with the ordering and spacing of the $\Lambda p_{3/2}$ and $\Lambda p_{1/2}$ states in $_\Lambda^{13}$C measured with a NaI counter array [22].

The energy-level spacings discussed above are not very sensitive to the tensor interaction. Consequently, for the derivation of the other three parameters (Δ, S_Λ, and S_N), T was assumed to be in the range of values of 0.01–0.06 MeV predicted using ΛN interactions from the Nijmegen one-boson-exchange (OBE) models (NSC97f, NSC89, ND, and NF) in G-matrix calculations [14,23]. With T taken to be

0.030 MeV, the remaining ΛN parameters that fit almost perfectly the four bound excited states of $^{7}_{\Lambda}$Li [24] are (parameters in MeV)

$$\Delta = 0.430, \quad S_{\Lambda} = -0.015, \quad S_{N} = -0.390. \quad (2)$$

C. The ΛN tensor interaction

Among the four ΛN spin-dependent interactions, only direct information on the ΛN tensor interaction has not been obtained experimentally. The derivation of the tensor interaction strength is important not only to complete the set of parameters but also to remove the theoretical assumption implicit in the derivation of the other three parameter values.

The strong NN tensor interaction is well understood by one-pion exchange, reduced at short distances by ρ exchange. But in the case of ΛN, these exchanges are forbidden because of the zero isospin of the Λ. The corresponding pseudoscalar K and vector K^* exchanges are allowed but cancel strongly because their masses are more similar than those of the π and the ρ [14]. As a result, the OBE models predict small strengths for the tensor interaction. This, and a relatively small variation for different models, can be seen from Table XI of Ref. [4] for the Nijmegen hard- and soft-core models and from Table XX of Ref. [5] for the extended soft-core models.

The ground-state doublet spacings in $p_{1/2}$-shell hypernuclei have large contributions from the tensor interaction. For example, in the simplified jj coupling model [13,14], the ground-state doublet spacings of $^{16}_{\Lambda}$O and $^{14}_{\Lambda}$N are given by

$$E(1^{-}) - E(0^{-}) = -1/3\Delta + 4/3 S_{\Lambda} + 8T, \quad (3)$$

while the $3/2^{+}$, $1/2^{+}$ spacing in $^{15}_{\Lambda}$N is 1.5 times larger. In contrast, the spacing of the doublet based on the $p_{3/2}$-hole state of ^{15}O,

$$E(2^{-}) - E(1^{-}) = 2/3\Delta + 4/3 S_{\Lambda} - 8/5 T, \quad (4)$$

has a coefficient of T relative to Δ that is an order of magnitude smaller than for the $p_{1/2}$ doublet in Eq. (3).

However, the difficulty of determining the tensor interaction strength is due not only to its small value but also to the small spacings of the spin doublets for which T contributes strongly. Since T is expected to have a small positive value, and Δ has a relatively large positive value, the contributions of Δ and T are expected to cancel strongly in $p_{1/2}$-shell hypernuclei, as can be seen from Eq. (3). Hence the spacings are expected to be quite small, and the ordering of the states in a doublet can be uncertain. A small spacing also means that the lifetime of the upper member of a doublet may be long compared with the lifetime for weak decay ($\sim$200 ps). In this situation, the only safe way to measure a doublet spacing is to measure the energies of γ rays feeding both members of the doublet from a higher level.

D. Motivation for the ^{16}O$(K^{-}, \pi^{-}\gamma)^{16}_{\Lambda}$O reaction

To study the ΛN tensor interaction, the (K^{-}, π^{-}) reaction on ^{16}O is ideal because bound states of both $^{16}_{\Lambda}$O and $^{15}_{\Lambda}$N can be produced. Figure 1 shows the level schemes of $^{16}_{\Lambda}$O and
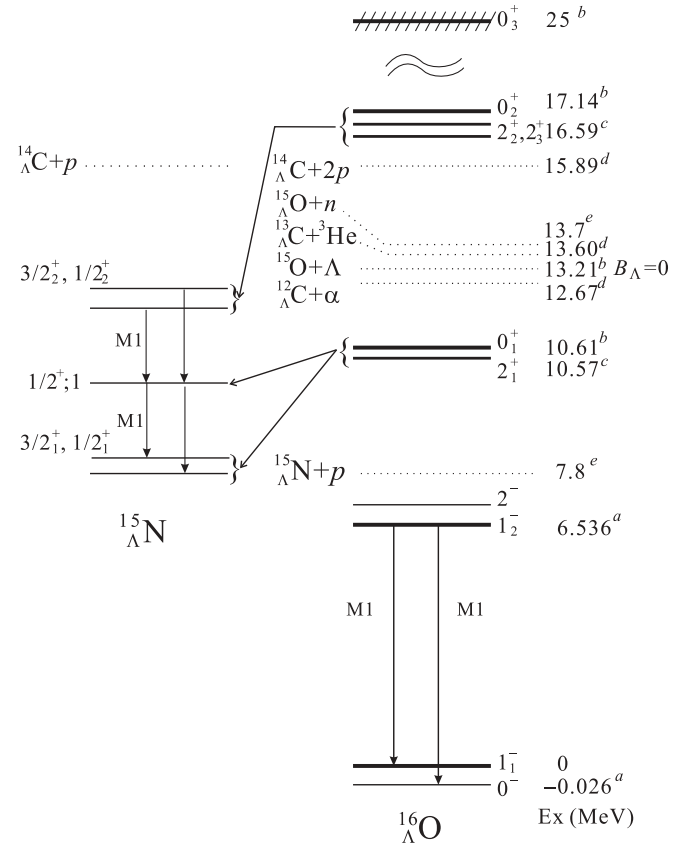

FIG. 1. Expected level schemes and γ-ray transitions of $^{16}_{\Lambda}$O and $^{15}_{\Lambda}$N from the ^{16}O(K^{-}, π^{-}) reaction. The 1^{-} states and 0^{+} states of $^{16}_{\Lambda}$O (thick lines) are most strongly populated by this reaction. The superscript a shows excitation energies from the present experiment, b from Ref. [19], and c from Ref. [27]. The particle-decay thresholds, except for $^{15}_{\Lambda}$N+p and $^{15}_{\Lambda}$O+n (see text), are determined from emulsion data [30] assuming $B_{\Lambda} = 13.21$ MeV for $^{16}_{\Lambda}$O. The 0^{+} and 2^{+} states in $^{16}_{\Lambda}$O can decay to all the low-lying $3/2^{+}$ and $1/2^{+}$ states in $^{15}_{\Lambda}$N via s- and d-wave proton emission.

$^{15}_{\Lambda}$N (the isospins of 1/2 for $^{16}_{\Lambda}$O and 0 for $^{15}_{\Lambda}$N are omitted). Predicted γ-ray transitions are also shown.

For kaon momenta less than 1 GeV/c, the (K^{-}, π^{-}) reaction proceeds predominantly by non-spin-flip ($\Delta S = 0$) transitions. Theoretical cross sections calculated in distorted-wave impulse approximation (DWIA) [25] for all the natural-parity states in Fig. 1 are shown in Fig. 2 for the incident kaon momentum used in the present experiment ($p_{K} = 900$ MeV/c). Substitutional states, in which a neutron is replaced by a Λ without changing the orbit, are strongly populated at forward angles ($\theta \leqslant 5^{\circ}$) via $\Delta L = 0$ transitions. The three 0^{+} states shown in Fig. 1 are of this nature (see below) and were observed, along with the two 1^{-} states ($\Delta L = 1$), at CERN [19]. The excitation energies given for the 0^{+} states in Fig. 1 come from a reanalysis of the CERN data [26]. The 1^{-} and 2^{+} ($\Delta L = 2$) states are seen strongly in the ^{16}O$(\pi^{+}, K^{+})^{16}_{\Lambda}$O reaction [27,28] and can be produced in the (K^{-}, π^{-}) reaction at larger angles (see Fig. 2). The excitation energies of the 2^{+} states are taken from Ref. [28], while the energies of the negative-parity states come from the
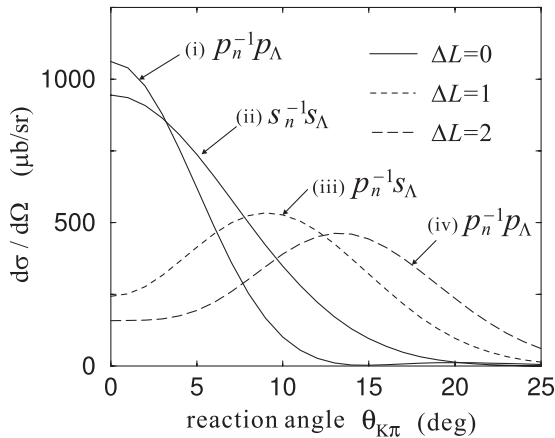
FIG. 2. Angular distributions, calculated in the DWIA [25], for the $^{16}O(K^-, \pi^-)^{16}_\Lambda O$ reaction at $p_K = 900$ MeV/c as a function of the laboratory reaction angle $\theta_{K\pi}$. The cross sections are for the (i) 0_1^+, (ii) 0_3^+, (iii) 1_2^-, and (iv) $2_2^+ + 2_3^+$ states shown in Fig. 1. For the 0_2^+, 1_1^-, and 2_1^+ states, the cross sections for (i), (iii), and (iv) should be multiplied by 1.65, 0.61, and 0.60, respectively. These different angular distribution patterns will be used later in Secs. V A 2 and V B 2 for the assignment of observed γ transitions.

present experiment [29]. The thresholds in Fig. 1 depend on the Λ binding energies (B_Λ values) for the hypernuclei involved, and these are not reliably determined from emulsion data [30] (few events with ambiguous interpretations).

The negative-parity states of $^{16}_\Lambda O$ in Fig. 1 have dominant $p_n^{-1}s_\Lambda$ configurations, whereas the positive-parity states have $p_n^{-1}p_\Lambda$ configurations except for the 0_3^+ state. The 0_1^+ and 0_2^+ states are the p-substitutional states, while the 0_3^+ state has an $s_n^{-1}s_\Lambda$ configuration and is the s-substitutional state. Both 1^- states in Fig. 1 are particle bound. The 6.6-MeV excited 1_2^- state is expected to decay to both ground-state doublet members $(1_1^-, 0^-)$ by $M1$ transitions. The upper level of the ground-state doublet is expected to decay to the lower level by a spin-flip $M1$ transition. However, for a small spacing of less than 100 keV, the detection efficiency of Hyperball becomes small. In addition, the weak decay of Λ in nuclei ($t_{1/2} \sim$ 200 ps) would compete with the $M1$ transition for a spacing of less than 100 keV. Thus, we need to detect both γ rays, $1_2^- \rightarrow 1_1^-$ and $1_2^- \rightarrow 0^-$, and determine the doublet spacing from the energy difference between these γ rays. The spin ordering of the doublet can be determined from the branching ratio for these γ transitions. Since the spin-flip cross section is expected to be much smaller than the non-spin-flip one, the yield of γ transitions from the 2^- state, which should decay mainly to the 1_1^- state by an $M1$ transition, is expected to be small.

It has been pointed out [31] that bound states of $^{15}_\Lambda N$ can be produced following proton emission from particle-unbound states in $^{16}_\Lambda O$. The proton-emission threshold of $^{16}_\Lambda O$ is expected to be at about $E_x \sim 7.8$ MeV based on systematics for the difference of the B_Λ values for $^{16}_\Lambda O$ and $^{15}_\Lambda N$. Making the same approximation and adding the 5.9 MeV between the neutron and proton thresholds in ^{15}O gives $\sim$13.7 MeV for the neutron-emission threshold in $^{16}_\Lambda O$.

The full $1\hbar\omega$ wave functions for the positive-parity states of $^{16}_\Lambda O$ contain admixtures of the following types of configu-

rations:

$$\alpha|(s^4 p^{11})p_\Lambda\rangle + \beta|(s^4 p^{10}sd)s_\Lambda\rangle + \gamma|(s^3 p^{12})s_\Lambda\rangle. \quad (5)$$

These states can decay by the s- and d-wave proton emission to the positive-parity states in $^{15}_\Lambda N$ via the $(s^4 p^{10}sd)s_\Lambda$ components in their wave functions. The lowest five-positive parity states of $^{15}_\Lambda N$ are shown in Fig. 1. For the same reason as in $^{16}_\Lambda O$, direct observation of the spin-flip $M1$ transition between the ground-state doublet members may not be possible. Therefore, to observe γ rays from $^{15}_\Lambda N$, the upper-doublet ($3/2_2^+$, $1/2_2^+$) or the $1/2^+$; 1 state should be produced. The 1^+ state at $E_x = 3.95$ MeV in ^{14}N, which is the core level for the upper doublet, decays by $M1$ transitions to the 0^+; 1 state at $E_x = 2.31$ and the ground 1^+ state with the branching rate of 100:4. Therefore, the cascade $M1$ transitions $(3/2_2^+, 1/2_2^+) \rightarrow 1/2^+$; 1 and $1/2^+$; $1 \rightarrow (3/2_1^+, 1/2_1^+)$ are likely to be observed in $^{15}_\Lambda N$.

The baryonic decay rates of the $p_n^{-1}p_\Lambda$ states ($0^+, 2^+$) have been calculated in the translationally invariant shell model (TISM) [32]. The predictions are that 12% of the 0_1^+ state decays to the $1/2^+$; 1 state, and 28% of the 0_2^+ state to the $1/2_2^+$ state. The $2_{2,3}^+$ states are calculated to decay mainly to the $3/2_2^+$ state.

Measurement of the ground-state doublet spacings in $^{16}_\Lambda O$ and/or $^{15}_\Lambda N$ determines a relationship between the values of Δ and T from the full shell-model version (which includes Λ-Σ coupling) of Eq. (3). A determination of the energies of more excited states of $^{16}_\Lambda O$ and $^{15}_\Lambda N$ tests the previously determined spin-dependent interaction strengths. In particular, the excited-state doublet in $^{15}_\Lambda N$ is based on a mainly $^3S_1$ core state, such as the ^6Li ground state, and the doublet spacing should be large and determined mainly by Δ.

II. EXPERIMENT

A. Principles

The γ-ray spectroscopy experiment E930('01) on $^{16}_\Lambda O$ and $^{15}_\Lambda N$ was carried out using the D6 beamline [33] at the BNL Alternating Gradient Synchrotron (AGS) for a period of two months in the fall of 2001.

Both $^{16}_\Lambda O$ and $^{15}_\Lambda N$ were produced via the $^{16}O(K^-, \pi^-)$ reaction with the γ rays being detected by a large-acceptance germanium (Ge) detector array called Hyperball. Incident and outgoing meson momenta were measured by magnetic spectrometers, and γ-ray spectra were obtained by selecting events corresponding to the $^{16}_\Lambda O$ mass region.

B. The (K^-, π^-) reaction and spectrometers

A side view of the detection apparatus is shown in Fig. 3. The D6 beamline [33] provided a high-purity and high-intensity K^- beam. The incident K^- momentum was set to 0.93 GeV/c. The energy loss in the beamline detectors and the target medium reduced the momentum to 0.91 GeV/c at the reaction point. This K^- momentum was chosen for a balance between hypernuclear production yield and Doppler shift effects. The repetition rate of the beam spill was 4.6 s,
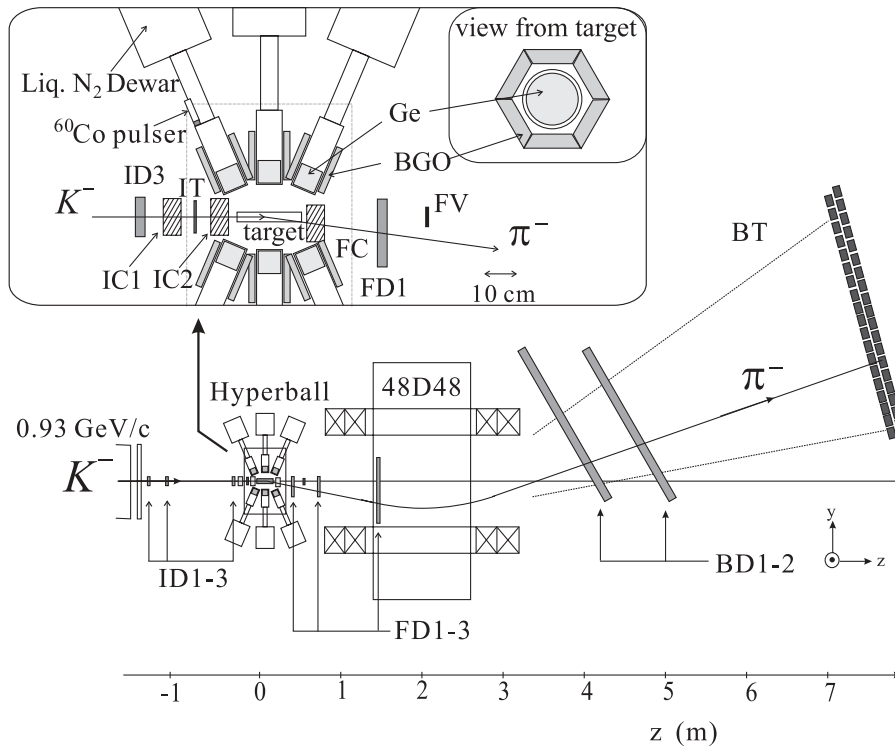
FIG. 3. Schematic view of the experimental setup (side view). The 48D48 is a dipole magnet; ID's, FD's, and BD's are drift chambers; IT, FV, and BT are plastic scintillation counter hodoscopes with IT and BT used to measure time of flight; and IC1, IC2, and FC are aerogel Čerenkov counters with $n = 1.03$. The Hyperball consisted of 14 sets of Ge detectors, each surrounded by six BGO counters. A ^{60}Co pulser was used to monitor the Ge detector live time between the beam-on and beam-off periods and consisted of a 1 kBq ^{60}Co source encapsulated together with a plastic scintillation counter. γ-ray events were selected by hits in a Ge detector without hits in the BGO counters. The 20 g/cm^2 H$_2$O target was irradiated with 4×10^{10} kaons.

and the beam duration time was 1.5 s. In each spill, 2×10^{13} 21 GeV/c protons bombarded the primary platinum target, and a K^- beam with a typical K^-/π^- ratio of 3 was delivered with a typical intensity of 2×10^5. In total, 4×10^{10} kaons were incident on the 20 g/cm^2 water target (hereafter "target" denotes the water target).

The incident K^- momentum was measured in the downstream part of the D6 beamline (not shown in the figure) using the transport matrix with information from a hit position in the plastic scintillation counter hodoscope before the last bending magnet and a straight track measured by three drift chambers (ID1–3) after it. See Ref. [33] for details.

The spectrometer for scattered particles consisted of a dipole magnet 48D48, which has a pole size of 48×48 in. and a gap size of 80 cm. It accepted scattering angles from $-8°$ to $8°$ in the horizontal direction and from $-16°$ to $0°$ in the vertical direction. The scattered particles were bent vertically (upward). The momentum was measured by the 48D48 and five drift chambers located upstream (FD1–3) and downstream (BD1–2) of the 48D48. In the present experiment, the 48D48 was operated at $0.8T$, optimized to the outgoing π^- momentum of about 0.8 GeV/c. The field distribution of the 48D48 used in track reconstruction analysis was calculated by the TOSCA code.

The (K^-, π^-) reaction events were selected in the trigger level by threshold-type aerogel Čerenkov counters (AC) with $n = 1.03$ located upstream (IC1 and IC2) and downstream (FC) of the target, and by time of flight (TOF) in the off-line analysis. Plastic scintillation counters MT (located upstream of the last bending magnet of the beamline and not drawn in the figure), IT, and BT were used to measure the TOF; and IT was used as a timing reference counter for all the detectors. MT is a horizontally segmented hodoscope, and BT is a vertically

segmented hodoscope. The typical flight lengths between corresponding TOF counters were 15 m (MT–IT) for incident and 7.9 m (IT–BT) for scattered particles, respectively. A plastic scintillation counter (FV), which covered a scattering angle less than 3° was located 50 cm downstream from the target and used to reject unscattered beam particles and very forward scattered particles in the trigger level. Events with small reaction angles were also rejected in the off-line analysis, because the vertex resolution is not enough to select reaction events in the target. The target was installed between the two AC's (IC2 and FC) spaced as closely as possible to minimize kaon decay events occurring in the target region. Such decay events contribute to the background but cannot be eliminated in the off-line analysis because their momentum range overlaps with that of hypernuclear production. The incident particle identification with two stages of AC's (IC1 and IC2) provided an almost pure K^- trigger but caused a kaon suppression of 4%. The efficiency of the outgoing particle identification by an AC (FC) for pions was 98%, and the misidentification of kaons as pions was 1%. However, such kaons were rejected by the FV.

C. γ-ray detector, Hyperball

Hyperball consisted of 14 sets of Ge detectors with bismuth germanate (BGO) scintillation counters. A typical configuration and size of the Ge detector and the BGO elements are shown in Fig. 3. Each Ge detector was surrounded by six BGO detectors of 19 mm radial thickness. Each Ge detector had an N-type coaxial crystal of about 7×7 cm ϕ and a relative efficiency to a 3×3 in. NaI counter of 60%. The BGO counters were used to suppress such background

events as Compton scattering, π^0 decay, and high-energy charged particles. The background from $K^- \to \pi^- \pi^0$ decay was particularly serious. Each Ge detector was equipped with a transistor-reset type preamplifier and connected to a shaping amplifier with a gated integrator (ORTEC 973U [34]). This solved the difficulty of operating the Ge detectors in a high counting rate and high energy-deposit rate environment. We also used timing filter amplifiers (ORTEC 579 [34]) for timing information.

The end cap of each Ge detector facing the beam was located at a distance of 10 cm from the beam axis. The Ge crystals covered a total solid angle of $0.25 \times 4\pi$ sr from the target center. The total photo-peak efficiency in the beam-on period was measured using γ-ray peaks from γ-cascade decays originating in the target and was determined to be $(1.5 \pm 0.3)\%$ for 2.3 MeV γ rays and $(4.2 \pm 1.0)\%$ for 0.7 MeV γ rays after including all electronics dead times and all analysis efficiencies. The efficiency curve as a function of the energy was simulated by the GEANT code, and the absolute scale was adjusted to fit the measured efficiencies. The relative efficiency for the beam-on and beam-off periods was measured by the monitoring system using triggerable 1 kBq ^{60}Co sources, each embedded in a plastic scintillator connected to a photo-multiplier tube (PMT) and installed behind a Ge detector as shown in Fig. 3 (^{60}Co pulser). These monitoring data were taken during both beam-on and beam-off periods with the scintillator detecting e^- from β decay and the corresponding Ge detector detecting γ rays in coincidence. The beam-on/beam-off efficiency ratio for each detector was measured to be $(90 \pm 5)\%$. Two γ-ray sources, ^{152}Eu and ^{60}Co, were used for energy calibration. However, the γ-ray energies of available sources were limited to 6.13 MeV, while the γ-ray energies from $^{16}_{\Lambda}$O are expected to be around 6.6 MeV. Therefore, we also used γ rays from activities (^{16}N, ^{14}O, ^{24}Na, and ^{75}Ge$_m$) produced by the beam in the target and surrounding materials. In particular, we used γ-ray peaks following ^{16}N(β^-) decay at 6129 and 7115 keV and their escape peaks. The ^{16}N was most likely produced by the ^{16}O(n, p) reaction on ^{16}O in the target and surrounding BGO detectors. These γ rays were observed in the Ge-self-trigger data taken during the beam-off period. Energy calibration was performed in the range from 0.1 to 7.1 MeV. The peak shifts between the beam-on and beam-off periods and the long-term gain shift were also corrected. The shift between beam-on/off was typically 1 keV, and the long-term shift was 2 keV at maximum.

The response function of the γ-ray peak shape after summing up the spectra of the 14 Ge detectors was found to be described as a Gaussian function up to 6.1 MeV. The beam-on energy resolution was 5.7 keV full width at half maximum (FWHM) for 2-MeV γ rays and 8.6 keV for 6.6-MeV γ rays. The energy calibration error was found to be 1.0 keV at 2 MeV and 1.5 keV for over 5 MeV.

D. Data taking and triggers

The K^- beam trigger was defined as $K_{in} = IT \times \overline{IC1} \times \overline{IC2}$. The π^- scattering trigger was defined as $PI_{out} = FC \times$ $\overline{FV} \times BT$. The data were taken according to the (K^-, π^-) trigger defined as $KPI = K_{in} \times PI_{out}$. The trigger rate was typically 1.1×10^3 per spill. To reduce the trigger rate, a second-level trigger was made using information on the Ge detector hits. When none of the Ge detectors had hits, data were not taken. The second-level trigger rate was typically 0.3×10^3 per spill.

Analog-to-digital converter (ADC) and time-to-digital converter (TDC) data were collected via four FASTBUS crates for all the detectors except for the Ge detectors, and via FERA bus for Ge detectors, to the corresponding VME memory modules (UMEM [35]) on an event-by-event basis. The accumulated data were read out by the host computer (a LINUX PC) in every beam-off period and recorded on a DVD RAM after being processed by the host computer.

Another type of data, triggered only by the Ge detectors (Ge-single-trigger data), was also taken in the beam-off period of every synchrotron cycle. These data were used for energy calibration of the Ge detectors.

III. DATA ANALYSIS: (K^-, π^-) REACTION

A. Hypernuclear masses

The $^{16}_{\Lambda}$O mass ($M_{^{16}_{\Lambda}O}$) was reconstructed as a missing mass in the ^{16}O(K^-, π^-) reaction. The binding energy of a Λ in the hypernucleus is defined by

$$B_\Lambda = M_{^{15}O} + M_\Lambda - M_{^{16}_{\Lambda}O}, \qquad (6)$$

where $M_{^{15}O}$ and M_Λ are the masses of the core nucleus (^{15}O) in its ground state and the Λ, respectively.

The absolute mass scale was calibrated using the π^0 mass reconstructed from the $K^- \to \pi^- \pi^0$ decay. The energy losses of the K^- and the π^- in the target medium were corrected event by event. In the present experiment, the mass resolution was 15 MeV (FWHM). We selected events with a reaction angle larger than $2°$ and a reaction vertex point in the target region.

Figure 4 shows the missing-mass spectrum from the ^{16}O(K^-, π^-) reaction plotted against the Λ binding energy (B_Λ) for those events accompanying γ rays with energies in the range of 1.5–7.0 MeV. As shown in Fig. 1, four narrow states (1_1^-, 1_2^-, 0_1^+, and 0_2^+) and one broad state (0_3^+), corresponding to the $s_N^{-1} s_\Lambda$ substitutional state at around $-B_\Lambda = 12$ MeV [19], are expected to be produced. However, they cannot be resolved in the missing-mass spectrum because of the limited mass resolution.

To observe the $^{16}_{\Lambda}$O γ rays, the mass region corresponding to the 1_2^- state was selected. The mass of the 1_2^- state is near $B_\Lambda = 7$ MeV from previous experiments [19,27,36]. Consequently, the 1_2^- state region was defined by $-17 < -B_\Lambda < 3$ MeV. The 20-MeV gate width corresponds to 88% of all the 1_2^- state events for the 15-MeV resolution. On the other hand, to observe the $^{15}_{\Lambda}$N γ rays, a mass region including the 0^+ and 2^+ states ($p_n^{-1} p_\Lambda$-state region) was selected. The 0_1^+ and 0_2^+ states are at $B_\Lambda = 2$ and -4 MeV [19], as are the 2_1^+ and $2_{2,3}^+$ states [27]. Therefore, we defined this region to be $-12 < -B_\Lambda < 14$ MeV, and this gate width covers 94% of
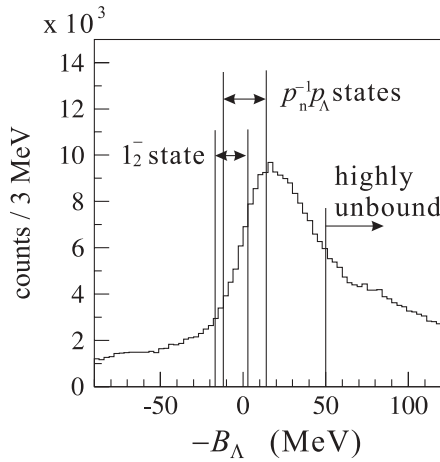
FIG. 4. Missing-mass spectrum for the ^{16}O(K^-, π^-) reaction plotted against the Λ binding energy (B_Λ) for those events accompanying γ rays with energies of 1.5–7.0 MeV. The indicated regions show the definitions of the 1^-_2 state region ($-17 < -B_\Lambda < 3$ MeV), the $p_n^{-1}p_\Lambda$ states region ($-12 < -B_\Lambda < 14$ MeV), and the highly unbound region ($-B_\Lambda > 50$ MeV).

the events for the 0^+_1 and 0^+_2 states. We also defined the highly unbound region as $-B_\Lambda > 50$ MeV. These defined regions are shown in Fig. 4.

B. Kinematical conditions

Figure 5 shows the acceptance, obtained by a Monte Carlo simulation, of the scattered-particle spectrometer as a function of the reaction angle $\theta_{K\pi}$. The momentum transfer q (MeV/c)
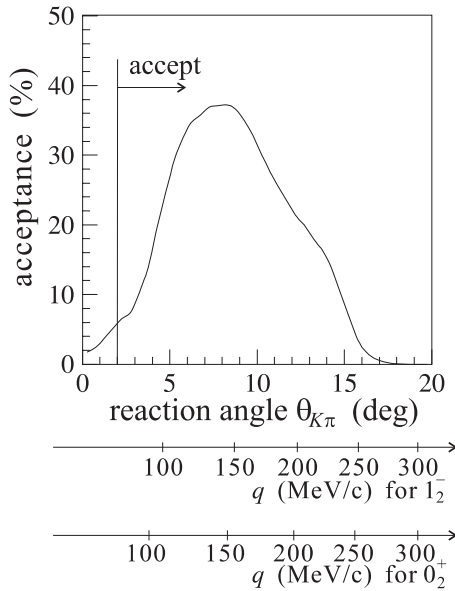

FIG. 5. Simulated reaction angle ($\theta_{K\pi}$) dependent acceptance of the scattered-particle spectrometer. Differences in acceptance for the 1^-_2 ($E_x = 6.6$ MeV) and 0^+_2 ($E_x = 17.1$ MeV) states of $^{16}_\Lambda$O are negligibly small. Momentum transfers q (MeV/c) for these states corresponding to the reaction angles are also shown. Events with reaction angles less than 2° were rejected in the off-line analysis.

corresponding to $\theta_{K\pi}$ is also shown. We simulated the cases of producing the $E_x = 6.6$ MeV (1^-_2) and 17.1 MeV (0^+_2) states. Differences in the q-dependent acceptances for these states were found to be negligibly small. The K^- momentum at the reaction point was distributed around 0.91 GeV/c with a width of 0.06 GeV (FWHM) on account of the original beam momentum spread and energy loss in the thick target.

As is evident from Fig. 2, the cross sections for the 0^+, 1^-, and 2^+ states formed via the ^{16}O(K^-, π^-) $^{16}_\Lambda$O reaction at $p_{K^-} = 900$ MeV/c peak at 0°, 9°, and 13°, respectively. Taking into account the angular distribution of these reactions and the spectrometer acceptance, the initial recoil momenta of $^{16}_\Lambda$O for the 1^-_2 and 0^+_2 states were estimated to be in the range of 100–250 and 100–200 MeV/c, respectively. The recoil momentum of $^{15}_\Lambda$N was also calculated to be in the range of 0–250 MeV/c assuming that the proton was emitted isotropically. The corresponding stopping times of these hypernuclei in the target medium were calculated using the SRIM code [37] to be in the range of 1.5–2.5 and 0–2 ps, respectively.

IV. DATA ANALYSIS: γ RAYS

A. Event selection for γ rays

Because the timing of a Ge detector hit with respect to the beam timing (IT hit) varies with γ-ray energy, the timing gate width was set as a function of energy. The gate width was 50 ns for 0.5 MeV, 30 ns for 2 MeV, and 20 ns for over 5 MeV. The gate width for the BGO counters was set to be 50 ns so as to achieve efficient background suppression without oversuppression from accidental coincidences.

To observe and identify statistically weak γ-ray peaks, the background level should be minimized. When gating the particle-unbound region, we found a lot of γ rays, such as ^{27}Al and ^{56}Fe γ rays around the 2 MeV region, originating from (n, n') reactions in the detector and surrounding materials. Since the neutrons were assumed to reach these materials a few ns after the triggered timing, we made another TDC cut which was used only to identify these γ rays. Figure 6(a) shows a TDC spectrum for a typical Ge detector plotted for γ-ray energies over 1.5 MeV. The timing cut conditions, prompt and delayed, were defined as shown in Fig. 6(a). Figures 6(b) and 6(c) show γ-ray spectra plotted for the highly unbound region in $^{16}_\Lambda$O with the prompt and delayed timing cuts, respectively. γ rays from the target materials are enhanced in the prompt spectrum in Fig. 6(b), and γ rays from the detector materials are enhanced in the delayed spectrum in Fig. 6(c).

B. γ-ray Doppler shifts

The energies of the expected γ rays from $^{16}_\Lambda$O and $^{15}_\Lambda$N are larger than 1 MeV except for the spin-flip transitions within the spin doublets. They are all $M1$ transitions, so their lifetimes are expected to be much shorter than, or of the same order as, the stopping time of the recoiling hypernucleus. Therefore, each γ-ray peak has a Doppler-broadened shape determined by the lifetime of the state, the stopping time, the response
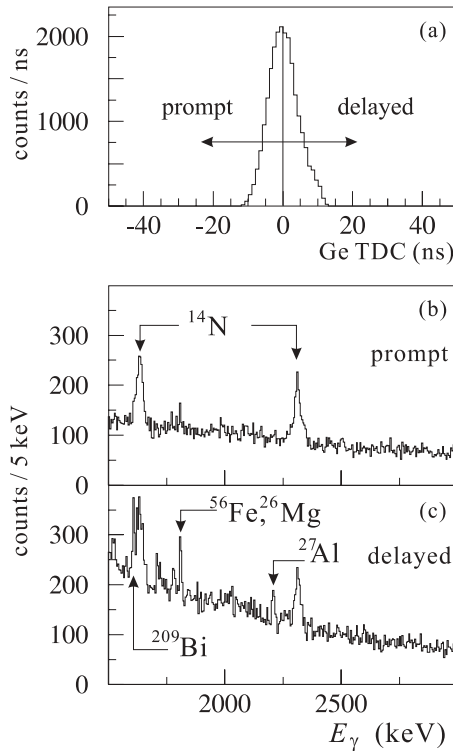
FIG. 6. (a) TDC spectrum for a typical Ge detector plotted for γ-ray energies over 1.5 MeV. (b) and (c) are the γ-ray energy spectra plotted for the highly-unbound region in $^{16}_{\Lambda}$O with the prompt and delayed timing cuts shown in (a), respectively.

function of the γ ray, and the kinematical conditions of the experiment.

1. Doppler-shift correction

When the lifetime of the initial state is much shorter than the stopping time, $\tau \lesssim 0.1$ ps, the γ-ray peak shape is fully broadened by the Doppler-shift effect. If we know the velocity of the recoiling hypernucleus (β) and the angle between the hypernuclear velocity and γ-ray emission (θ) in the laboratory frame, the shifted γ-ray energy can be corrected by use of the relativistic formula

$$E_{\gamma}(\text{cor.}) = E_{\gamma} \frac{1 - \beta \cos\theta}{\sqrt{1 - \beta^2}}, \qquad (7)$$

where $E_{\gamma}(\text{cor.})$ and E_{γ} are the Doppler-shift corrected energy and the measured energy, respectively. The direction of γ-ray emission in the laboratory frame was calculated from the reaction vertex point and the position of the Ge crystal with a hit. The velocity β and direction of the hypernucleus were calculated from the kaon and pion momentum vectors measured by the incident and outgoing particle spectrometers.

First, we consider the Doppler-shift correction for $^{16}_{\Lambda}$O γ rays. Since the γ-ray energies of $M1$ transitions from the 1^-_2 state are larger than 6 MeV, the lifetime of the state is expected to be very short, because the lifetime of the corresponding core level ($3/2^-$) is very short (<2.5 fs). Figure 7 shows the
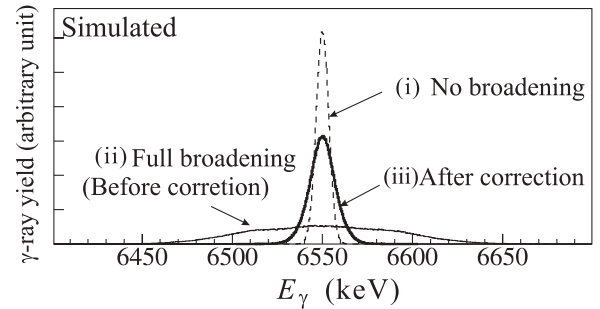

FIG. 7. Simulated peak shapes of γ rays emitted from recoiling $^{16}_{\Lambda}$O, produced by the ^{16}O (K^-, π^-) reaction, assuming a γ-ray energy of 6.55 MeV. The figure shows (i) not broadened (original response function), (ii) fully Doppler-broadened (before correction), and (iii) Doppler-shift-corrected peak shapes.

simulated γ-ray peak shapes of $^{16}_{\Lambda}$O assuming an original energy of 6.55 MeV, giving (i) the original response function, (ii) the fully Doppler-broadened shape, and (iii) the shape after Doppler-shift correction for (ii).

Second, we consider the Doppler-shift correction for $^{15}_{\Lambda}$N γ rays. The lifetimes of the upper-doublet states ($3/2^+_2$, $1/2^+_2$) in $^{15}_{\Lambda}$N are expected to be a few fs [15]. The recoil velocity and the recoil direction of $^{15}_{\Lambda}$N are changed from those of $^{16}_{\Lambda}$O due to the proton emission. However, since the mass of the secondary nucleus $^{15}_{\Lambda}$N is not so different from the mass of primary nucleus $^{16}_{\Lambda}$O and the emitted proton energy is small, the Doppler-shift correction can be also applied to the secondary nucleus. We simulated a Doppler-shift-corrected γ-ray peak shape for $^{15}_{\Lambda}$N using a simulated β for $^{16}_{\Lambda}$O(0^+_2), assumed to be produced according to the calculated angular distribution (see Fig. 2). Proton emission was assumed to be isotropic. We found that the Doppler-shift correction makes a broadened peak narrower and square-shaped. Figure 8 shows the simulated γ-ray peak shapes assuming that a 2-MeV γ ray is emitted from $^{15}_{\Lambda}$N following proton emission: (i) fully Doppler-broadened and (ii) Doppler-shift-corrected peak shapes.

In addition, we also simulated other decay processes such as $^{13}_{\Lambda}$C+^{3}He and $^{12}_{\Lambda}$C+α. In these cases, it was found that the correction does not make the Doppler-broadened peak shapes narrower.

In these simulations, we assumed that hypernuclei emit γ rays isotropically in the center-of-mass frame. Although angular correlations are expected to exist between the scattered π^- and γ rays [38], the effect on the corrected energy is simulated to be negligibly small.

2. Doppler-shift attenuation method

Information on the lifetime of a state can be obtained by analyzing the partly Doppler-broadened peak shape. This is called the Doppler-shift attenuation method (DSAM). In particular, when the stopping time and the lifetime are of the same order of magnitude, DSAM can be used to determine the lifetime. This method was first applied for hypernuclei
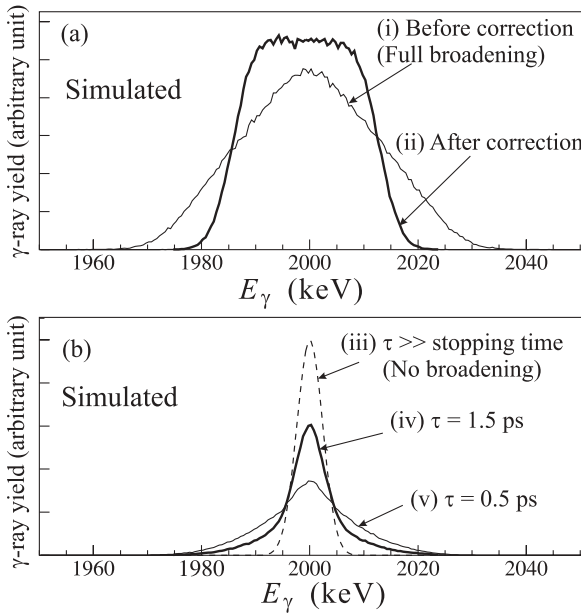
FIG. 8. Simulated peak shapes for 2-MeV γ rays from $^{15}_\Lambda$N following proton emission from the $^{16}_\Lambda$O(0^+_2) state produced via the ^{16}O (K^-, π^-) reaction. Figure (a) shows the (i) fully Doppler-broadened and (ii) Doppler-shift-corrected peak shapes. Figure (b) shows the lifetime dependence of the peak shape, (iii) $\tau \gg$ stopping time (no broadening, original response function), (iv) $\tau = 1.5$ ps, and (v) $\tau = 0.5$ ps.

to determine the $B(E2)$ value of the $5/2^+$ excited state of $^7_\Lambda$Li [39].

DSAM can also be applied to the secondary hypernuclei if the recoil momentum is known. Among the states to be produced, the $^{15}_\Lambda$N($1/2^+$; 1) state is expected to have a lifetime of the same order as the stopping time ($\sim$2 ps), an estimate

for the lifetime of the state being 0.5 ps [15]. However, the absolute mass of $^{15}_\Lambda$N is not well determined, and the $^{15}_\Lambda$N production rates from the 0^+_1, 0^+_2, and s-substitutional states of $^{16}_\Lambda$O cannot be obtained because of the limited mass resolution. These ambiguities are included in the systematic errors. The ambiguities mainly stem from the Q value of the $^{16}_\Lambda$O$\rightarrow$ $^{15}_\Lambda$N $+ p$ decay. Details are given later.

In the simulation, we assumed that $^{16}_\Lambda$O decays isotropically to $^{15}_\Lambda$N and a proton in the center-of-mass frame. The simulated γ-ray peak shape is shown in Fig. 8(b), which shows the lifetime-dependent peak shape for (iii) $\tau \gg$ stopping time (no broadening, original response function), (iv) $\tau = 1.5$ ps, and (v) $\tau = 0.5$ ps.

V. RESULTS

Some results for the $^{16}_\Lambda$O γ rays have already been reported in Ref. [29], which focused on the determination of the ground-state doublet spacing in $^{16}_\Lambda$O. In this paper, details of the results on the $^{16}_\Lambda$O γ rays and additional results on the $^{15}_\Lambda$N γ rays are discussed.

A. γ rays from $^{16}_\Lambda$O

1. γ-ray spectrum

Figure 9 shows the mass-gated γ-ray energy spectra around 6 MeV in coincidence with the ^{16}O(K^-, π^-) reaction at $\theta_{K\pi} > 2°$; Fig. 9(a) is plotted for the highly-unbound region ($-B_\Lambda > 50$ MeV) without Doppler-shift correction; Fig. 9(b) is for the 1^-_2-state region ($-17 < -B_\Lambda < 3$ MeV) without Doppler-shift correction, and Fig. 9(c) is for the 1^-_2 state region with Doppler-shift correction. Here, the Doppler-shift correction was applied assuming that γ rays were emitted before the
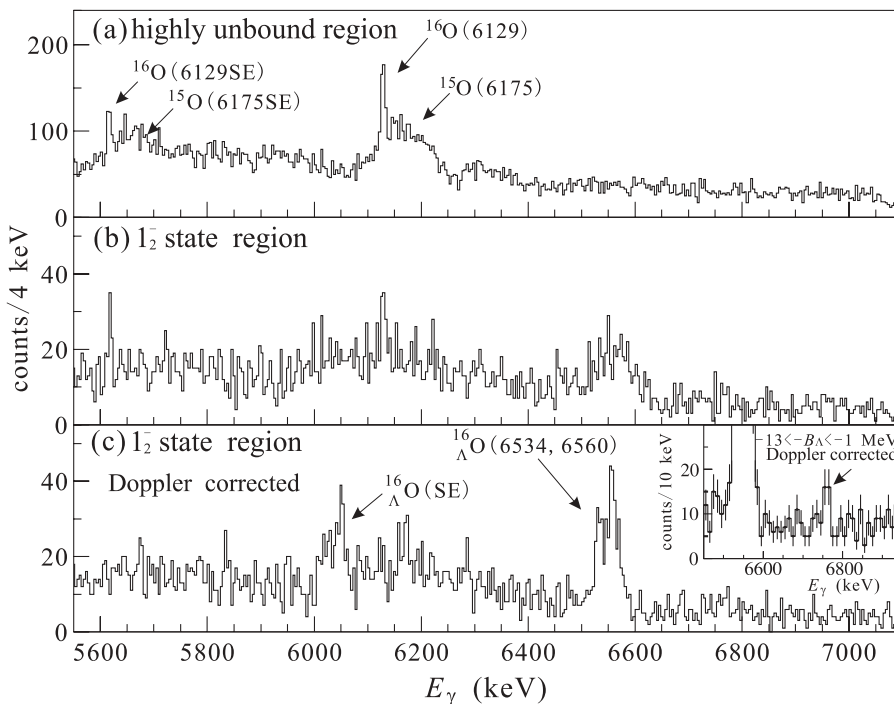

FIG. 9. Mass-gated γ-ray spectra measured in the ^{16}O(K^-, π^-) reaction at $\theta_{K\pi} > 2°$ for (a) the highly unbound region ($-B_\Lambda > 50$ MeV), (b) the 1^-_2 state region ($-17 < -B_\Lambda < 3$ MeV), and (c) the same spectrum as in (b) but with event-by-event Doppler-shift corrections applied. A structure around 6.5–6.6 MeV in (b) becomes two narrow peaks after Doppler-shift correction. The two peaks are assigned as $M1(1^-_2 \rightarrow 1^-_1, 0^-)$ transitions. Single-escape (SE) peaks from these $M1$ transitions can also be seen in (c), and likewise SE γ-ray peaks from ^{15}O(6175 keV) and ^{16}O(6129 keV) in (a). Inset in (c) shows the Doppler-corrected spectrum for a narrower mass cut ($-13 < -B_\Lambda < -1$ MeV) which is set to maximize the signal-to-noise ratio for the 6534- and 6560-keV γ-ray peaks. A gathering of events with a statistical significance 3σ from background appears at 6758 keV.

recoiling hypernucleus slowed down. The highly unbound and the 1_2^- state regions are defined in Fig. 4.

We found ^{16}O(6129 keV) and ^{15}O(6175 keV) γ-ray peaks in the spectra for both the highly unbound region [Fig. 9(a)] and the 1_2^--state region [Fig. 9(b)]. On the other hand, a bump around 6.6 MeV was found only in the spectrum for the 1_2^--state region, and it becomes two narrow peaks after the Doppler-shift correction, as shown in Fig. 9(c). The peaks are attributed to $M1$ transitions from the 1_2^- state to both ground-state doublet members $(1_1^-, 0^-)$ in $^{16}_\Lambda$O because the 1_2^- state is the only bound state, other than the 1^- member of the ground-state doublet, that can be strongly populated by the reaction, and γ-ray peaks from other (hyper)nuclei cannot become so narrow after Doppler-shift correction (Fig. 8). This argument is supported by the fact that the shape of the bump before Doppler-shift correction in Fig. 9(b) is consistent with the fully Doppler-broadened peak shape [Fig. 7(b)]. In addition, the structure observed at ~6.04 MeV in Fig. 9(c) has a shape similar to the $^{16}_\Lambda$O peaks at ~6.55 MeV and corresponds to their single-escape (SE) peaks.

We made a fit to the Doppler-shift-corrected spectrum with the simulated peak shape [Fig. 7(c)] assuming that the background around a full-energy peak has two components: one is constant for the whole region below and above the γ-ray energy (E_0), and the other is caused by multiple Compton scattering and exists only on the lower energy side with the form $a + bE$ for $E < E_0$ and 0 for $E > E_0$. In a simulation taking into account the Doppler-shift correction, the step-function was smoothed around $E = E_0$ and then used in the fitting. We obtained for the lower peak an energy of 6533.9 ± 1.2(stat) ± 1.7(syst) keV and a yield of $127 \pm 15 \pm 5$ counts; and for the upper peak, $6560.3 \pm 1.1 \pm 1.7$ keV and $183 \pm 16 \pm 5$ counts. The systematic errors include the calibration error and the accuracy of the Doppler-shift correction. The excitation energy of the 1_2^- state becomes 6561.7 keV after applying the nuclear recoil correction to the γ-ray energy. The energy difference between the two γ rays, $26.4 \pm 1.6 \pm 0.5$ keV, corresponds to the ground-state doublet spacing. The relative intensities of the γ rays are

$$\frac{I_\gamma(6534)}{I_\gamma(6560)} = 0.69 \pm 0.11 \pm 0.10, \tag{8}$$

where the γ-ray efficiencies were assumed to be the same.

We also found a gathering of events at 6760 keV in the 1^- state region spectrum [Fig. 9(c)]. To reduce the background, we set a narrower mass gate $(-13 < -B_\Lambda < -1$ MeV) to maximize the signal-to-noise ratio, S^2/N, for the 6534- and 6560-keV γ-ray peaks. Then, we found a peak with a statistical significance of 3σ $(21.0^{+7.2}_{-6.5}$ counts) at an energy of $6758 \pm 4 \pm 4$ keV, as shown in the inset of Fig. 9(c). The peak width was found to be consistent with the simulated Doppler-shift-corrected peak shape. Applying the same mass gate, the sum of the $1_2^- \to 1_1^-, 0^-$ γ-ray yields was found to be 262 ± 24 counts. The γ-ray intensity ratio was

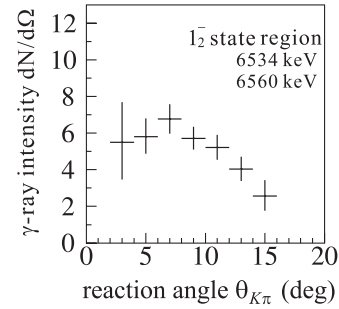$$\frac{I_\gamma(6758)}{I_\gamma(6534) + I_\gamma(6560)} = 0.08 \pm 0.03. \tag{9}$$

FIG. 10. Reaction angle ($\theta_{K\pi}$) dependence of the $^{16}_\Lambda$O γ-ray intensities (sum of the 6534- and 6560-keV γ rays) from the 1_2^- state in $^{16}_\Lambda$O measured in the ^{16}O(K^-, π^-) reaction for the 1_2^- state region $(-17 < -B_\Lambda < 3$ MeV) defined in Fig. 4. Shown are the γ-ray counts divided by the solid angle taking into account the spectrometer acceptance (Fig. 5).

2. Angular distributions

Figure 10 shows the reaction angle ($\theta_{K\pi}$) dependence for the sum of the 6534- and 6560-keV γ rays observed from the 1^- state region, $-17 < -B_\Lambda < 3$ MeV, defined in Fig. 4. The sum of these γ-ray yields were obtained from a fit using the simulated peak shape with the two γ-ray energies and the ratio of the two γ-ray yields fixed to be 0.69 from Eq. (8). The γ-ray intensity was obtained from the summed γ-ray yield divided by a solid angle taking into account the angular dependence of the spectrometer acceptance (Fig. 5). The observed angular distribution agrees well with the calculated distribution in Fig. 2 for a $\Delta L = 1$ transition and is thus consistent with the state that emits the 6534- and 6560-keV γ rays being the 1_2^- state.

3. Level assignments

The branching ratio $I_\gamma(1^- \to 1^-)/I_\gamma(1^- \to 0^-)$ is 0.5 in the weak-coupling limit and 0.41 when the level mixing is taken into account [15]. The measured relative intensity of the 6534- and 6560-keV γ rays [Eq. (8)] should therefore give information on the spin ordering of the doublet members. First, a correction has to be made for the fact that the effective γ-ray efficiency of the Hyperball is different for the two transitions due to angular distribution effects. For pure $M1$ transitions and a forward reaction angle ($\theta_{K\pi} \sim 0°$) [38],

$$W(\theta_{\pi\gamma}) \propto \begin{cases} (1 + \cos^2\theta_{\pi\gamma}) & \text{for} \quad (1^- \to 1^-), \\ (1 - \cos^2\theta_{\pi\gamma}) & \text{for} \quad (1^- \to 0^-), \end{cases} \tag{10}$$

where $\theta_{\pi\gamma}$ is the angle between the π^- and the γ ray. The Ge detectors were not arranged isotropically with respect to the π^- direction, and effective efficiencies were calculated from a simulation with the result $\varepsilon(1^- \to 1^-)/\varepsilon(1^- \to 0^-) = 0.80 \pm 0.05$(syst.). The error comes from ambiguities in the real size and shape of the Ge detectors. Since we measured the hypernuclear production events at finite angles, the actual ratio is larger than this estimation. Taking into account the $\pi\gamma$ correlation, the expected branching ratios of 0.41 or 0.50 should be corrected to 0.33 or 0.40. Thus, the measured ratio of $0.69 \pm 0.11 \pm 0.10$ is slightly larger than expected but still
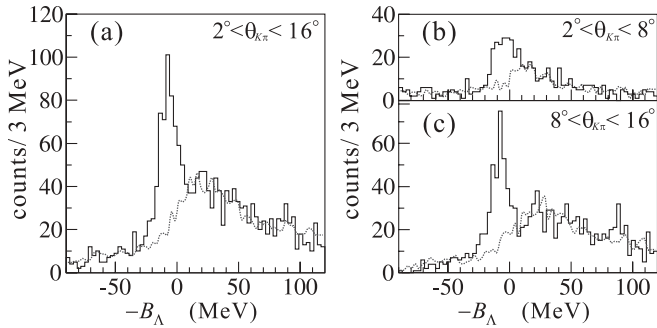
FIG. 11. Missing-mass spectra measured in the ^{16}O(K^-, π^-) reaction plotted against the Λ binding energy (B_{Λ}) for events accompanying a γ ray with $E_{\gamma}(\text{cor.}) = 6500$–$6600$ keV for (a) $2° < \theta_{K\pi} < 16°$, (b) $2° < \theta_{K\pi} < 8°$, and (c) $8° < \theta_{K\pi} < 16°$. The dotted lines show the expected background shapes plotted for events accompanying γ rays with $E_{\gamma}(\text{cor.}) = 6600$–$7000$ keV and scaled to fit the background region $(-90 < -B_{\Lambda} < -40$ MeV$)$.

favors a 0^- assignment for the lower level of the ground-state doublet.

The intensity of the 6758-keV γ ray is much weaker than those of the transitions from the 1^-_2 state [Eq. (9)]. With the caveat that 2^+ hypernuclear states based on the 6.793-MeV $3/2^+$ or 6.859-MeV $5/2^+$ levels of ^{15}O could possibly be excited through small $p^{-1}p_{\Lambda}$ components in their wave functions [cf. Eq. (5)], this γ-ray transition is tentatively attributed to the $M1(2^- \to 1^-_1)$ transition from the 2^- member of the $p_{3/2}^{-1}s_{\Lambda}$ doublet, giving an excitation energy of $6786 \pm 4 \pm 4$ keV for the 2^- state. If this assignment is correct, this is the first experimental data to identify directly produced spin-flip and non-spin-flip states in Λ hypernuclei.

4. Missing-mass spectrum

Figure 11 shows missing-mass spectra as a function of Λ binding energy (B_{Λ}) for events accompanying a γ ray with a Doppler-shift-corrected γ-ray energy $E_{\gamma}(\text{cor.}) = 6500$–$6600$ keV corresponding to the $1^-_2 \to 1^-_1, 0^-_1$ transitions. In Fig. 11(a), a prominent peak is observed corresponding to the experimental value of $-B_{\Lambda} = -7$ MeV for the 1^-_2 state. By fitting this peak in with a Gaussian, the mass resolution was determined to be 15 ± 1 MeV. The mass resolutions obtained by fitting the mass spectra in Figs. 11(b) and 11(c) were 15 ± 2 MeV.

5. Lifetime analysis

The fully broadened γ-ray peak shape contains information on the lifetime. We fitted the Doppler-shift-uncorrected spectrum with simulated peak shapes for various lifetimes using the measured γ-ray energies and yield ratio. Then, we obtained an upper limit for the lifetime of the 1^-_2 state in $^{16}_{\Lambda}$O of $\tau < 0.3$ ps at the 68% confidence level.

B. γ rays from $^{15}_{\Lambda}$N

1. γ-ray spectrum

Figure 12 shows the mass-gated γ-ray spectra measured in coincidence with the ^{16}O(K^-, π^-) reaction; Figs. 12(a) and 12(c) are plotted for the highly unbound region $(-B_{\Lambda} > 50$ MeV$)$; Figs. 12(b), 12(d), and 12(e) are for the $p_n^{-1}p_{\Lambda}$-states region $(-12 < -B_{\Lambda} < 14$ MeV$)$. Event-by-event Doppler-shift corrections are applied for Fig. 12(e). The highly unbound and $p_n^{-1}p_{\Lambda}$-states regions are defined in Fig. 4.

A prominent peak is found at 2268 keV in the spectrum in Fig. 12(d) which is gated on the $p_n^{-1}p_{\Lambda}$-states region. The γ-ray peak is taken to be hypernuclear, since there are no γ-ray transitions of this energy in ordinary nuclei with $A \leqslant 16$. The γ-ray peak has two components, namely, a narrow part and a Doppler-broadened part, which indicates that the lifetime of this transition is close to the stopping time of ~ 1 ps for the hypernucleus in the target. There are four candidates for secondary hypernuclei with thresholds below the $^{16}_{\Lambda}$O(0^+_2) state, namely, $^{15}_{\Lambda}$N, $^{15}_{\Lambda}$O, $^{13}_{\Lambda}$C, and $^{12}_{\Lambda}$C (see Fig. 1). The long lifetime of the 2268-keV γ ray suggests that the corresponding core transition is also slow, thus leaving the 0^+; 1, first-excited state of ^{14}N ($E_x = 2.31$ MeV, $\tau = 98$ fs) as the only candidate. Moreover, the excitation energies of members of the first-excited doublets in $^{12}_{\Lambda}$C and $^{13}_{\Lambda}$C are known to be 2.51 MeV for $^{12}_{\Lambda}$C(1^-_2) [40] (2.63 MeV from KEK E336 [28]) and 4.88 MeV for $^{13}_{\Lambda}$C$(3/2^+)$ [22] (4.85 MeV [28]). The unknown first-excited state of $^{15}_{\Lambda}$O must be based on the 5.17-MeV 1^- state of ^{14}O, and the 0^+_2 state of $^{16}_{\Lambda}$O cannot decay to a state at this high an energy. Therefore, the 2268-keV γ-ray peak is attributed to $^{15}_{\Lambda}$N. In addition, two broad peaks at 1960 and 2440 keV can be seen in Fig. 12(d), and they become square-shaped narrower peaks in Fig. 12(e) after the Doppler-shift correction. These peak shapes are consistent with the result of the simulation for $^{15}_{\Lambda}$N described in Sec. IV B1 [see Figs. 8(a) and 8(b)]; while, according to the simulation, γ-ray peaks from $^{12}_{\Lambda}$C and $^{13}_{\Lambda}$C cannot become narrower. Therefore, these two γ rays are also attributed to transitions in $^{15}_{\Lambda}$N. On the other hand, a narrow γ-ray peak observed at 2215 keV can be attributed to a part of the broad γ-ray peak from ^{27}Al$(n, n'\gamma)$, because it is clearly enhanced by the "delayed" TDC cut [see Fig. 6].

As shown in Fig. 12(b), no prominent peak corresponding to the ground-state spin-flip $M1$ transition is observed in the region from 100 to 700 keV. The sensitivity for such a peak and the ground-state doublet spacing will be discussed later (Sec. V B6).

We made fits for the Doppler-shift-corrected γ-ray spectrum using the simulated peak shape from Fig. 8(a). We obtained energies of $1960.7^{+1.2}_{-1.7} \pm 1.7$ and $2442.0^{+0.7}_{-1.7} \pm$ 1.7 keV, with corresponding yields of $190^{+30}_{-36} \pm 5$ and $313 \pm 35 \pm 5$ counts. For the narrow peak, we obtained the energy of $2267.6 \pm 0.3 \pm 1.5$ keV and a yield of $744 \pm 39 \pm 15$ counts. The detailed fitting procedure for the 2268-keV γ ray is described later. The measured γ-ray energies correspond to transition energies of 1960.8, 2267.8, and 2442.3 keV. Taking into account the energy dependence of the γ-ray efficiency, the relative γ-ray intensities for the $p_n^{-1}p_{\Lambda}$-states region were
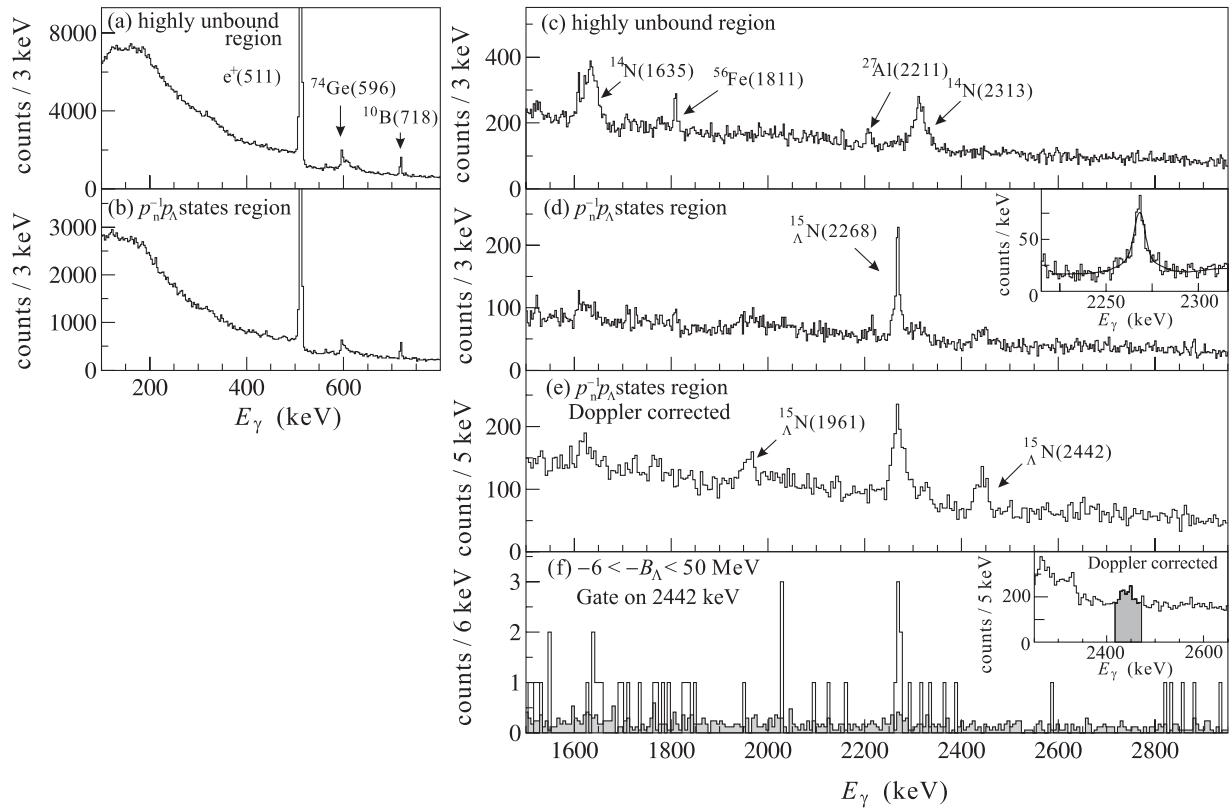
FIG. 12. Mass-gated γ-ray spectra from the (K^-, π^-) reaction on the 20 g/cm^2 H$_2$O target. (a) and (c) are plotted for the highly unbound region $(-B_\Lambda > 50$ MeV); (b), (d), and (e), for the $p_n^{-1} p_\Lambda$-states region. (e) is the spectrum with event-by-event Doppler-shift corrections applied to (d). Three γ-ray peaks, a narrow peak at 2268 keV in (d) and Doppler-broadened peaks at 1961 and 2442 keV in (d), which become narrower peaks in (e), are assigned as γ rays from $^{15}_\Lambda$N. (f) is a γ-γ coincidence spectrum plotted for $-6 < -B_\Lambda < 50$ MeV. The solid line is the spectrum of γ rays accompanied by another γ ray with E_γ(cor.) = 2442 ± 25 keV, as shown in the inset. The shaded region in (f), which shows the background level, is the spectrum of γ rays accompanied by another γ ray with E_γ(cor.) = 2600–4000 keV, and with the counts scaled to the γ-ray counts at 2442 ± 25 keV.

found to be

$$I_\gamma(1961) : I_\gamma(2268) : I_\gamma(2442) = 0.23^{+0.04}_{-0.05} : 1 : 0.45 \pm 0.05. \tag{11}$$

Figure 12(f) shows the spectrum of γ rays emitted in coincidence with another γ ray with a Doppler-corrected energy of E_γ(cor.) = 2442 ± 25 keV for the $^{16}_\Lambda$O mass range of $-6 < -B_\Lambda < 50$ MeV. The shaded region in Fig. 12(f) shows the expected background, which is derived from the spectrum of γ rays accompanied by another γ ray with E_γ(cor.)= 2600–4000 keV for the same mass region, with the counts scaled to the counts in the 2442 ± 25 keV gate corresponding to the shaded region in the inset of Fig. 12(f). The mass region $-6 < -B_\Lambda < 50$ MeV was set to select the 0_2^+ state $(-B_\Lambda = 4$ MeV) and higher states. A peak with 6 counts appeared at 2268 keV, the energy of one of the other γ rays from $^{15}_\Lambda$N. The probability for 6 events to appear in the narrow region specified by 2268 ± 12 keV from a random fluctuation of the background of 1.2 ± 0.3 counts was estimated to be 0.4% using a Poisson distribution. Thus the possibility of a background fluctuation was rejected. Since the peak shapes indicate that the lifetime of the 2442-keV transition is shorter than that of the 2268-keV transition, the

decay chain γ (2442 keV) $\rightarrow \gamma$ (2268 keV) was determined. The yield of the 2442-keV γ ray for the $-6 < -B_\Lambda < 50$ MeV region was obtained to be $330 \pm 47 \pm 10$ counts, and the expected yield of the 2268-keV γ ray in coincidence is estimated to be 4.6 counts if no other transition strongly competes with the 2268-keV transition. Therefore, the 6 counts with 1.2 ± 0.3 counts background is consistent with the expected coincidence yield. On the other hand, no excess of events was found in the γ-γ coincidence spectrum with the 1961-keV γ ray, consistent with the lower yield of the 1961-keV γ ray.

2. Angular distributions

Figure 13 shows the reaction angle ($\theta_{K\pi}$) dependence of the $^{15}_\Lambda$Nγ-ray intensities for the $p_n^{-1} p_\Lambda$-states region in the ^{16}O(K^-, π^-) reaction. The γ-ray intensities were obtained from the measured γ-ray counts divided by the spectrometer acceptance (Fig. 5) and normalized to the relative efficiency for the 6550-keV γ ray. The panels of the figure show the distributions for the 2268-, 2442-, and 1961-keV γ rays. The spectra in Figs. 13(a) and 13(b) show forward-peaking angular distributions with a significant intensity remaining at large
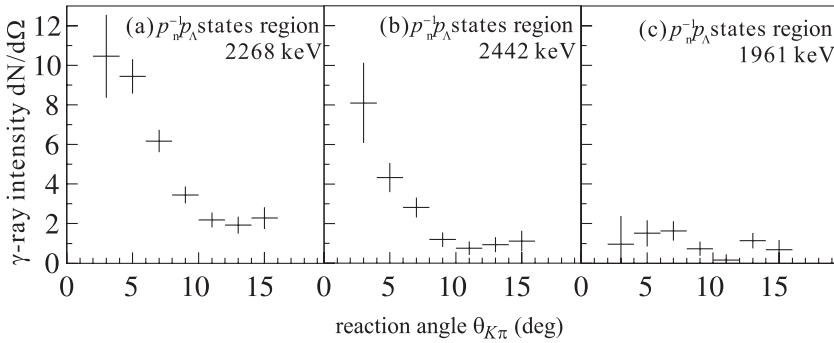
FIG. 13. Reaction angle ($\theta_{K\pi}$) dependence of the $^{15}_{\Lambda}$N γ ray intensities measured in the ^{16}O(K^-, π^-) reaction for the $p_n^{-1}p_\Lambda$-states mass region ($-12 < B_\Lambda < 14$ MeV) in $^{16}_{\Lambda}$O. The panels show the relative intensities of (a) 2268-keV, (b) 2442-keV, and (c) 1961-keV γ rays. Relative intensities were obtained by dividing the measured γ-ray counts by the spectrometer acceptance (Fig. 5). The relative γ-ray efficiencies are normalized to that of the 6550-keV γ ray.

angles ($\theta_{K\pi} > 10°$). This indicates that the $^{15}_{\Lambda}$N excited states deexcited by the 2268- and 2442-keV γ rays are produced mainly by proton emission from $^{16}_{\Lambda}$O states excited by $\Delta L = 0$ transitions with some contribution from states produced by $\Delta L = 2$ transitions. On the other hand, the $^{15}_{\Lambda}$N excited state leading to the 1961-keV γ deexcitation is mainly produced from nonsubstitutional states excited by $\Delta L \geqslant 1$ transitions.

3. Level assignments

The partly broadened shape of the 2268-keV γ-ray peak indicates a lifetime comparable to the stopping time of ~ 1 ps. Since the ^{14}N($0^+; 1 \rightarrow 1^+; 0$) transition has a lifetime of 0.10 ps and an energy of 2313 keV, the 2268-keV γ ray is attributed to a $^{15}_{\Lambda}$N transition corresponding to this core transition, namely, from the $1/2^+; 1$ state to one of the ground-state doublet members ($3/2^+, 1/2^+$). In the weak-coupling limit, the $B(M1)$ values for the decay to the $3/2^+$ and $1/2^+$ states would be in the ratio of 2:1. However, taking into account the level mixing, they are calculated to be in the ratio of 10:1 [15]. Therefore, the 2268-keV γ ray is taken to correspond to the $1/2^+; 1 \rightarrow 3/2_1^+$ transition.

The lowest state in ^{14}N that decays to the $0^+; 1$ state (the core level of the $1/2^+; 1$ state in $^{15}_{\Lambda}$N) is the 3948-keV 1^+ state, and it gives rise to the $3/2_2^+, 1/2_2^+$ doublet. Therefore, the initial state for the 2442-keV γ-ray transition is most likely to be one of these doublet members. The $\Delta L = 0$ dominance shown in the angular distribution [Fig. 13(b)] indicates that the 2442-keV γ ray mostly stems from the $^{16}_{\Lambda}$O(0_2^+) state or the $0s$-hole state (see Fig. 1). The TISM calculation [32] suggests that the $^{15}_{\Lambda}$N($1/2_2^+$) state, rather than the $^{15}_{\Lambda}$N($3/2_2^+$) state, is dominantly produced from the $^{16}_{\Lambda}$O(0_2^+) state. On this basis, the 2442-keV γ ray is likely to be the $1/2_2^+ \rightarrow 1/2^+; 1$ transition.

All the excited states higher than the $0^+; 1$ state in ^{14}N decay mainly to the $0^+; 1$ state or the $1^+; 0$ ground state. Since no other γ rays from $^{15}_{\Lambda}$N are observed, the 1961-keV γ-ray transition is also likely to be a transition decaying to the $1/2^+; 1$ state. The $\Delta L \neq 0$ dominance in the angular distribution [Fig. 13(c)] implies that the 1961-keV γ ray is predominantly emitted from a state populated by proton emission from the 2^+ states of $^{16}_{\Lambda}$O(2^+). The TISM calculation suggests that the 2^+ states in $^{16}_{\Lambda}$O decay to the $3/2_2^+$ state rather than the $1/2_2^+$ state. On this basis, the 1961-keV γ ray is likely to be the $3/2_2^+ \rightarrow 1/2^+; 1$ transition.

As described above, the $\theta_{K\pi}$ distributions of the 2442- and 1961-keV γ rays imply that the $1/2^+$ state is the upper member

and the $3/2^+$ state is the lower member of the excited doublet. Because the 3948-keV $1^+; 0$ state of ^{14}N is mainly ^3S in nature (see Sec. VI), the upper-doublet spacing is dominantly due to the spin-spin interaction term Δ; and for $\Delta > 0$ the spin antiparallel state becomes the lower level, as for $^7_\Lambda$Li($1/2^+$). The contradiction between the implications of the γ-ray yields as a function of pion reaction angle and the underling structure of $^{15}_{\Lambda}$N will be discussed in Sec. VI.

4. Missing-mass spectra

Figure 14 shows missing-mass spectra, plotted as a function of Λ binding energy (B_Λ), for the three γ rays attributed to $^{15}_{\Lambda}$N in the ^{16}O ($K^-, \pi^-\gamma$) reaction. The energy and angular ranges are specified in the caption.

By fitting the excess over the background with a Gaussian, the peak widths gated on the 2268-keV γ ray were found to be 21 ± 2, 19 ± 2, and 23 ± 3 MeV (FWHM) from Figs. 14(a), 14(b), and 14(c), respectively. These widths are significantly wider than the mass resolution. The natural widths of the $p_n^{-1}p_\Lambda$ states and the separations between the 0^+ and 2^+ states in each group of levels (see Fig. 1) are much smaller than the mass resolution (see Fig. 1) [19,27], suggesting that the $1/2^+; 1$ state in $^{15}_{\Lambda}$N is not produced from a single group of states in $^{16}_{\Lambda}$O. By comparing Fig. 14(b) with 14(c), more events are clearly seen at around 20–40 MeV in Fig. 14(c) showing that the $1/2^+; 1$ state of $^{15}_{\Lambda}$N is fed by proton emission decay from several states of $^{16}_{\Lambda}$O produced by $\Delta L > 0$ transitions.

On the other hand, the widths from Figs. 14(d), 14(e), and 14(f) were 17 ± 2, 17 ± 3, and 17 ± 5 MeV (FWHM), respectively. This suggests that the state which emits 2442 keV γ ray is dominantly produced from the 0_2^+ state and its partners in $^{16}_{\Lambda}$O.

The widths from Figs. 14(g), 14(f), and 14(i) were 26 ± 8, 26 ± 8, and 18 ± 9 MeV (FWHM), respectively, and no information on the population from states of $^{16}_{\Lambda}$O can be obtained.

5. Lifetime analysis

The lifetime of the $1/2^+; 1$ state was derived from the shape of the peak by fitting with the simulated shape. Since the recoil velocity is affected not by the absolute masses of $^{16}_{\Lambda}$O and $^{15}_{\Lambda}$N but by the Q value of the proton decay, it is necessary to know the masses of the $^{16}_{\Lambda}$O and $^{15}_{\Lambda}$N states contributing to the decay.

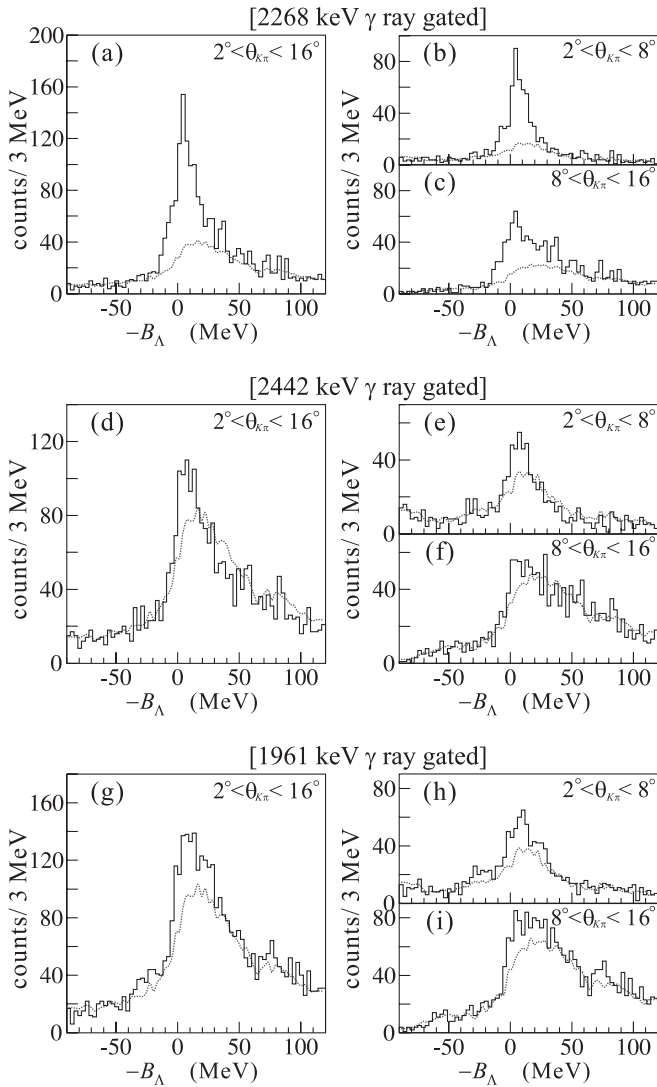FIG. 14. Missing-mass spectra for the ^{16}O(K^-, π^-) reaction as a function of Λ binding energy (B_Λ). The solid lines are plotted for those events accompanying γ rays in the energy range $E_\gamma = 2268 \pm 8$ keV for (a), (b), and (c), E_γ(cor.) $= 2442 \pm 16$ keV for (d), (e), and (f), and E_γ(cor.) $= 1961 \pm 16$ keV for (g), (f), and (i). The reaction angles covered are $2° < \theta_{K\pi} < 16°$ for (a), (d), and (g), $2° < \theta_{K\pi} < 8°$ for (b), (e), and (f), and $8° < \theta_{K\pi} < 16°$ for (c), (f), and (i). The dashed lines show the expected background shapes for the corresponding reaction angles, determined from the events accompanying γ rays with energies from 2500 to 3000 keV after scaling to fit the background region $(-90 < -B_\Lambda < -30 \text{ MeV})$.

In the simulation, we used the excitation energies of the 0^+, 2^+ states and the proton emission threshold as shown in Fig. 1. We assumed that all the excited states in $^{15}_\Lambda$N are produced directly from the excited 0^+ and 2^+ states at 17 MeV and that the 1961- and 2442-keV γ rays are from decays to the $1/2^+$; 1 state with the intensities in Eq. (11). Here, the lifetimes of the upper-doublet states were assumed to be much shorter than that of the $1/2^+$; 1 state, and their effect was neglected. This assumption is justified because the core state of the doublet $[^{14}$N$(1^+_2)]$ has a short lifetime (7 fs) compared to the scale set by the stopping time. The measured $\theta_{K\pi}$ distribution from Fig. 13(a) was used (cf. Fig. 2). In addition, the reaction angle was selected in the region from $2°$ to $8°$ to reduce the contributions from the nonsubstitutional states evident in the 20–40 MeV region of Fig. 14(c). The uncertainty in the excitation energies of states in $^{16}_\Lambda$O from previous experiments was found to have a negligible effect. The systematic error on the lifetime stems mainly from lack of knowledge of the decay ratio of the 0^+_1 and 0^+_2 states to the $1/2^+$; 1 state (± 0.2 ps). Uncertainty in the response function for the γ-ray peak at this energy was found to also contribute to the error in the lifetime (± 0.1 ps). Then, the lifetime obtained for the $1/2^+$; 1 state is 1.5 ± 0.3 (stat.) ± 0.3 (syst.) ps. This lifetime is 15 times longer than that of the 0^+; 1 core state and longer than the theoretically predicted value of 0.5 ps [15]. The reason for this dramatic increase in the lifetime of the hypernuclear state is discussed in Sec. VI.

We also examined the lifetimes of the initial states of the 1961- and 2442-keV γ rays by fitting the spectrum without Doppler-shift correction. In the simulation of the peak shape, we assumed that the $\theta_{K\pi}$ distributions were the same as that of the 2268-keV γ ray. Then the upper limits (68% C.L.) on the lifetimes were found to be $\tau < 0.2$ ps for the 1961-keV γ ray and $\tau < 0.3$ ps for the 2442-keV γ ray.

6. Ground-state doublet spacing

In Sec. V B3, the 2268-keV γ ray was taken to correspond to the $1/2^+$; $1 \to 3/2^+_1$ transition based on the theoretical expectation that this transition should be by far the stronger of the two possible γ rays deexciting the $1/2^+$; 1 level. The energy of the $1/2^+$; $1 \to 1/2^+_1$ transition would determine the ground-state doublet spacing, but no candidate is observed. In addition, no low-energy γ-ray peak corresponding to the ground-state doublet, spin-flip transition ($1/2^+_1 \to 3/2^+_1$ or $3/2^+_1 \to 1/2^+_1$) is observed. In these circumstances, nothing can be said about the ground-state doublet spacing if the $1/2^+$ state is the upper member of the doublet as the shell-model calculations predict (see Sec. VI).

If, on the other hand, the $3/2^+_1$ state is the upper level of the doublet, as expected in the the jj-coupling limit [14] given that $^{16}_\Lambda$O has a 0^- ground state, an upper limit can be put on the doublet spacing. The $B(M1)$ for the $3/2^+_1 \to 1/2^+_1$ transition can be estimated quite accurately in the weak-coupling limit [38] as

$$B(M1; 3/2^+_1 \to 1/2^+_1) = (g_\Lambda - g_c)^2/4\pi\mu_N^2, \quad (12)$$

where $g_c = 0.4038$ [41] and $g_\Lambda = -1.226$ [42]. Then, $\tau(3/2^+) = 0.269 \, E_\gamma^{-3}$ ps with E_γ in MeV. Taking into account the γ-ray efficiency and the competition between electromagnetic and weak decay ($\tau_{\text{weak}} \sim 200$ ps for most nuclei [43–45]) for the $3/2^+_1$ state, the sensitivity of the experiment is high enough to observe a γ-ray peak with $E_\gamma > 100$ keV even if the $3/2^+_1$ state was not produced from $^{16}_\Lambda$O directly. Then we can conclude that the ground-state doublet spacing in $^{15}_\Lambda$N would be
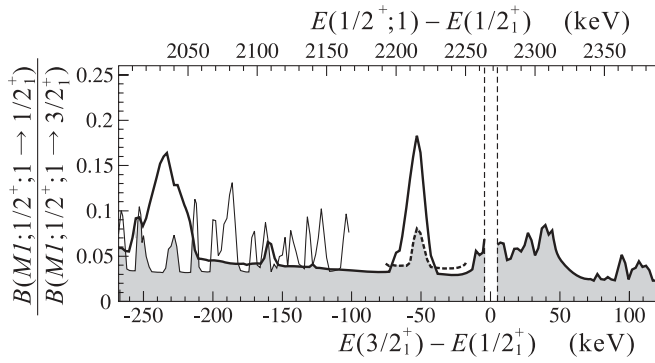
$$E(3/2^+_1) - E(1/2^+_1) < 100 \text{ keV}. \quad (13)$$

FIG. 15. Upper limit for the $B(M1)$ ratio between the $1/2^+; 1 \to 1/2^+_1$ and $1/2^+; 1 \to 3/2^+_1$ transitions as a function of the ground-state doublet spacing, $E(3/2^+_1) - E(1/2^+_1)$, and the $1/2^+; 1 \to 1/2^+_1$ transition energy. The thick line is the result of a peak search for the $1/2^+; 1 \to 1/2^+_1$ transition obtained by fitting the spectrum from 2000 to 2370 keV [Fig. 12(d)]. The dashed line is from the same procedure but with the "prompt" TDC cut. The thin line is the result of a peak search for the $1/2^+_1 \to 3/2^+_1$ transition obtained by fitting the spectrum from 100 to 270 keV [Fig. 12(b)].

7. The $1/2^+; 1 \to 1/2^+_1$ transition

As noted previously, no prominent γ-ray peak corresponding to the $1/2^+; 1 \to 1/2^+_1$ transition has been observed. An upper limit for the $B(M1)$ ratio between the $1/2^+; 1 \to 1/2^+_1$ and the $1/2^+; 1 \to 3/2^+_1$ transitions as a function of the ground-state doublet spacing can be obtained from the γ-ray spectrum. This is shown in Fig. 15, where the shaded region shows the allowed range of the $B(M1)$ ratio. The ratios in Fig. 15 were obtained from the upper limit of the γ-ray yield taking into account the relative γ-ray efficiencies.

The thick line shows the upper limit of the $B(M1)$ ratio obtained by fitting the spectrum from 2000 to 2370 keV assuming that the $1/2^+; 1 \to 1/2^+_1$ transition has the same γ-ray peak shape as the $1/2^+; 1 \to 3/2^+_1$ transition. The dashed line is obtained by fitting the spectrum with the "prompt" TDC cut to reduce the ^{27}Al(n, n') γ ray at 2211 keV. The thin line is obtained by fitting the spectrum from 100 to 270 keV, assuming that the $1/2^+_1 \to 3/2^+_1$ γ ray has the original response function because the lifetime of the $1/2^+_1$ state (half the estimate for the $3/2^+_1$ level in the previous subsection) is much longer than the stopping time and with the estimates for the electromagnetic and weak-decay lifetimes taken into account.

The $B(M1)$ ratio between the $1/2^+; 1 \to 1/2^+_1$ and $1/2^+; 1 \to 3/2^+_1$ transitions is calculated to be 10:1 with the level mixing taken into account [15] using the ΛN parameters from the first analysis of the $^{16}_{\Lambda}$O γ-ray data [29]. As shown in Fig. 15, either the doublet spacing is less than 5 keV or the upper limit on the $B(M1)$ ratio is $\sim$0.09 (the calculation puts the $1/2^+_1$ level $\sim$100 keV above the $3/2^+_1$ level). The interpretation of this result is discussed in detail in Sec. VI. Basically, small $1^+_2 \times s_\Lambda$ admixtures in the wave functions of the ground-state doublet members introduce strong destructive interferences from the strong $1^+_2; 0 \to 0^+; 1$ $M1$ core transition into the γ decays from the $1/2^+; 1$ level of $^{15}_{\Lambda}$N.
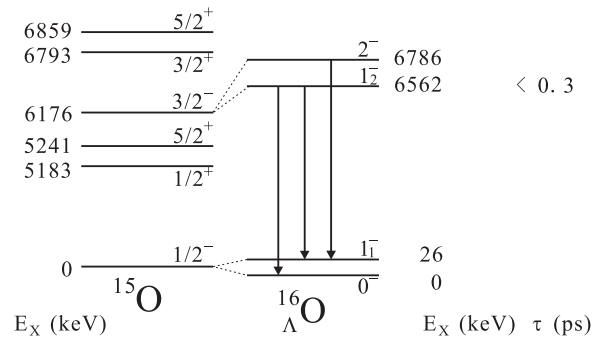

FIG. 16. Experimentally determined level scheme of $^{16}_{\Lambda}$O and observed γ-ray transitions. The corresponding level scheme of ^{15}O is also shown.

C. Summary of results

Figure 16 shows the experimentally determined level scheme of $^{16}_{\Lambda}$O. As shown in the figure, the excitation energies and spin ordering of both ground and 6.7-MeV excited doublets have been determined. This is the first determination of the spin ordering and the spacing of a $p_{1/2}$-shell hypernuclear ground-state doublet. In addition, this is the first observation of a spin-flip state (the 2^- state) that is directly produced via the (K^-, π^-) reaction.

Figure 17 shows the level scheme of $^{15}_{\Lambda}$N together with the corresponding core levels of ^{14}N [41]. Since the spin ordering and spacing of the ground-state doublet were not experimentally determined, the excitation energies are given as level spacings from the $3/2^+_1$ state. The existence of the 4710-keV excited state was determined from the coincidence of the 2442-keV γ ray with the 2268-keV γ ray. On the other hand, while the existence of the 4229-keV excited state was not unambiguously determined, the 1961-keV γ ray is likely a transition to the $1/2^+; 1$ state.

FIG. 17. Experimentally determined level scheme of $^{15}_{\Lambda}$N and observed γ-ray transitions (solid arrows). The corresponding level scheme of the ^{14}N core nucleus is also shown. Since the spin ordering of the ground-state doublet is not determined, the excitation energies of $^{15}_{\Lambda}$N are given as level spacings from the $3/2^+_1$ state. The existence of the 4229-keV excited state was not experimentally determined, but the 1961-keV γ ray is likely a transition to the $1/2^+; 1$ state.
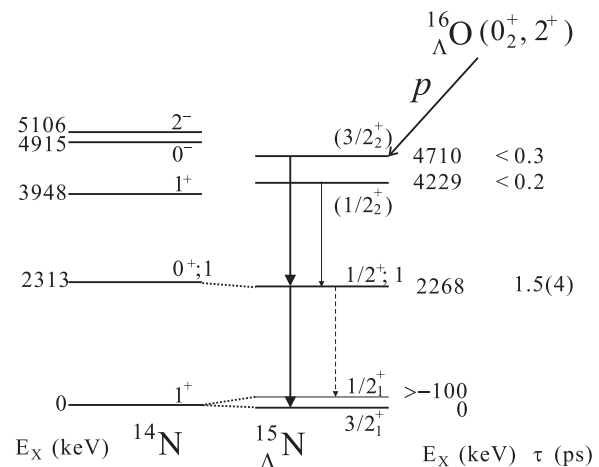
TABLE I. Observed hypernuclear γ rays by the (K^-, π^-) reaction. Intensities are normalized to the largest yield γ rays. The 2442- and 1961-keV γ ray transitions in $^{15}_\Lambda$N are not experimentally determined, but the most likely assignments are shown.

Gated mass (MeV)	E_γ (keV)	Counts	Relative intensity	$^A_\Lambda Z$	$(J_i; T_i \to J_f; T_f)$
$-17 < -B_\Lambda < 3$	$6560.3 \pm 1.1 \pm 1.7$	$183 \pm 16 \pm 5$	100	$^{16}_\Lambda$O	$1^-_2 \to 0^-$
	$6533.9 \pm 1.2 \pm 1.7$	$127 \pm 16 \pm 5$	$69 \pm 11 \pm 10$	$^{16}_\Lambda$O	$1^-_2 \to 1^-_1$
$-13 < -B_\Lambda < -1$	$6758 \pm 4 \pm 4$	$21.0^{+7.2}_{-6.5}$		$^{16}_\Lambda$O	$2^- \to 1^-_1$
	$2442.0^{+0.7}_{-1.7} \pm 1.7$	$313 \pm 35 \pm 5$	49 ± 5	$^{15}_\Lambda$N	$\to 1/2^+; 1$
$-12 < -B_\Lambda < 14$	$1960.7^{+1.2}_{-1.7} \pm 1.7$	$190^{+30}_{-36} \pm 5$	23 ± 5	$^{15}_\Lambda$N	$(\to 1/2^+; 1)$
	$2267.6 \pm 0.3 \pm 1.5$	$744 \pm 39 \pm 15$	100	$^{15}_\Lambda$N	$1/2^+; 1 \to 3/2^+; 0$

The observed γ-ray transitions are summarized in Table I.

VI. DISCUSSION

There are some uncertainties concerning the level assignments for the upper-doublet members in both hypernuclei. In $^{16}_\Lambda$O, the 6758-keV transition assigned as originating from the 2^- level has a statistical significance of 3σ (Sec. V A 3). Also, it cannot be completely ruled out that it comes from a positive-parity state (see Fig. 16) populated by a weak non-spin-flip, $\Delta L = 2$ transition in the (K^-, π^-) reaction. In $^{15}_\Lambda$N, the tentative assignments for the upper doublet shown in Fig. 17 are based on shell-model calculations using positive Δ values such as that in Eq. (2) (and in analogy to the ground-state doublet in $^7_\Lambda$Li). The γ-ray yields as a function of the reaction angle $\theta_{K\pi}$ (Sec. V B 3) suggest an inverted order for this doublet. However, the interpretation of these yields depends on an approximate $1\hbar\omega$ shell-model calculation [32] to estimate the population of states in $^{15}_\Lambda$N via proton emission from the 0^+ and 2^+ states of $^{16}_\Lambda$O (see the end of Sec. IV). These predictions depend on small amplitudes [the β in Eq. (5)] in the $^{16}_\Lambda$O wave functions, which are difficult to estimate reliably. Finally, from what is known on radiative decays in ^{14}N [41], it is difficult to see how any of the observed γ rays could originate from higher levels in $^{15}_\Lambda$N. In this section, then, we accept the level assignments made in Figs. 16 and 17 and compare the experimental results with theory.

As outlined in Sec. I A, the structure of p-shell Λ hypernuclei is interpreted in terms of shell-model calculations that include both $p^n s_\Lambda$ and $p^n s_\Sigma$ configurations. These calculations, including preliminary analyses of the present data, are described in Ref. [15] and in more detail in Ref. [46]. The $\langle p_N s_\Lambda | V | p_N s_\Sigma \rangle$ matrix elements were calculated from a multirange Gaussian potential (YNG interaction) fitted to G-matrix elements calculated for the SC97f(S) interaction [9]. Harmonic oscillator wave functions with $b = 1.7$ fm were used. These matrix elements were then multiplied by a factor of 0.9 to simulate the Λ-Σ coupling of the SC97e(S) interaction. This interaction is based on the NSC97e potential [4] which describes quite well the spacing of the 1^+ and 0^+ states of the $A = 4$ hypernuclei [9–12]. In the same parametrization as for

the ΛN interaction (see Sec. I A),

$$\bar{V}' = 1.45, \quad \Delta' = 3.04, \quad S'_\Lambda = S'_N = -0.09, \quad T' = 0.16 \tag{14}$$

characterize the five matrix elements (in MeV) for the Λ-Σ coupling interaction. This interaction [15] is kept fixed in the present analysis.

A. The $^{16}_\Lambda$O spectrum

From the shell-model calculations, the contribution from each of the ΛN parameters to a given eigenenergy can be calculated; and by taking differences, the coefficient of each parameter entering into an energy spacing can be deduced. These are given in the first line of Table II for each listed pair of levels in $^{16}_\Lambda$O. It can be seen that the coefficients of the parameters giving the two doublet spacings do not deviate much from those given in Eqs. (3) and (4) describing the simple jj-coupling limit. This is because the ΛN interaction is too weak to cause large mixing between the 1^- weak-coupling basis states with an unperturbed core separation energy of 6.176 MeV. In fact, the purity of the dominant basis state is never less than 99.7% for the states of interest in $^{16}_\Lambda$O and $^{15}_\Lambda$N. That is, the sum total of admixed Λ and Σ configurations is less than 0.3%. The downward energy shifts caused by Λ-Σ coupling are calculated to be 29, 61, 99, and 7 keV for the 0^-, 1^-_1, 1^-_2, and 2^- states, respectively, and these lead to the contributions to the energy spacings listed in the fourth column of Table II. The sum of the contributions from the ΛN parameters, the core energy difference, and the Λ-Σ coupling gives an accurate but not perfect (see below) representation of the energy-level spacings.

Assuming that the Λ-Σ coupling and the small value of $S_\Lambda = -0.015$ from $^9_\Lambda$Be data [see Sec. I B and Eq. (2)] are fixed, these expressions can be used to extract values for Δ, S_N and T. Since S_N affects only core separations and not the doublet spacings, the two measured doublet spacings in $^{16}_\Lambda$O (see Fig. 16) give a pair of simultaneous equations for Δ and T. The solution gives $\Delta = 0.312$ MeV and $T = 0.0248$ MeV. Here, Δ is derived from the excited-state doublet spacing in $^{16}_\Lambda$O because the main contributor of this doublet is Δ. On the other hand, the most important feature of the ground-state doublet splitting is the almost complete cancellation between

TABLE II. Energy spacings in $^{16}_{\Lambda}$O. ΔE_C is the contribution of the core level spacing (see Fig. 16). The first line in each case gives the coefficients of each of the ΛN effective interaction parameters as they enter into the spacing; the second line gives the actual energy contributions to the spacing in keV using the parameters in Eq. (15) which are derived from a fit to the measured level spacings in the final column. The calculated spacings are given in the penultimate column.

J_i^π	J_f^π	ΔE_C	$\Lambda\Sigma$	Δ	S_Λ	S_N	T	ΔE^{th}	ΔE^{exp}
1_1^-	0_1^-			-0.370	1.367	-0.002	7.888		
		0	-32	-107	-21	1	177	26	26
1_2^-	1_1^-			-0.260	-1.235	-1.495	-0.779		
		6176	-38	-75	19	489	-17	6536	6536
2_1^-	1_2^-			0.629	1.367	-0.003	-1.710		
		0	92	182	-21	1	-38	226	224

substantial contributions from T and Δ (aided by Λ-Σ coupling.) There is thus great sensitivity to the value of T.

Similarly, the difference between the centroid energies of the two doublets (or the energy separation between the 1^- levels), with a small correction for Λ-Σ coupling, gives $S_N = -0.322$ MeV; here, $l_N \cdot s_N$ simply augments the spin-orbit splitting of the hole states of the core nucleus ^{15}O.

A rediagonalization of the energy matrices with new parameters leads to small shifts in the energy levels and slightly changed values for the coefficients of the parameters in the expressions that give the energy-level differences. The parameter set (in MeV) that fits the measured energy-level spacings in $^{16}_{\Lambda}$O is then given by

$$\Delta = 0.290, \quad S_\Lambda = -0.015, \quad S_N = -0.327, \quad T = 0.0224. \tag{15}$$

The second line for each pair of levels in Tables II and III gives the actual breakdown of the contributions to the energy spacings for this parameter set. As mentioned above, all parameters except for S_Λ are derived only from the $^{16}_{\Lambda}$O levels. Nevertheless, Δ and S_N show smaller but similar values to those in Eq. (2) obtained from the $^{7}_{\Lambda}$Li levels.

It is to be noted that a 0.15% admixture of the 1^- basis state in $^{16}_{\Lambda}$O reduces the binding energy of the lower 1^- state by 10 keV (0.0015×6500) and vice versa for the upper state. This is the reason why the sum of the individual energy contributions in Table II (similarly in Table III) do not add up to precisely ΔE^{th}.

B. The $^{15}_{\Lambda}$N spectrum

In addition to the effective YN interaction, the structure of $^{15}_{\Lambda}$N is sensitive to details of the two-hole, p-shell wave functions for ^{14}N. The tensor interaction in the p-shell Hamiltonian used for the $^{15}_{\Lambda}$N calculation was kept fixed during a fit to 90 p-shell levels and was chosen to ensure cancellation in the Gamow-Teller matrix element for ^{14}C(β^-) decay. The relevant core wave functions in LS coupling are (these are p^{10} wave functions in a supermultiplet basis so that the phases differ from those for simple two-hole wave functions)

$$|^{14}\text{N}(1_1^+;0)\rangle = -0.1139\,^3S + 0.2405\,^1P - 0.9639\,^3D,$$
$$|^{14}\text{N}(1_2^+;0)\rangle = 0.9545\,^3S + 0.2958\,^1P - 0.0390\,^3D, \tag{16}$$
$$|^{14}\text{N}(0^+;1)\rangle = 0.7729\,^1S + 0.6346\,^3P,$$

TABLE III. Energy spacings in $^{15}_{\Lambda}$N. The core contributions ΔE_C to the energy spacings are derived from the excitation energies of the core 0^+; 1 and 1^+; 0 states at 2313 and 3948 keV (see Fig. 17). The first line in each case gives the coefficients of each of the ΛN effective interaction parameters as they enter into the spacing; the second line gives the actual energy contributions to the spacing in keV using the parameters in Eq. (15) which are derived from a fit to the $^{16}_{\Lambda}$O levels spacings. The full calculated and measured spacings are given in the final two columns. The parenthetic values correspond to spin assignments that are not experimentally determined but are the likely assignments.

$J_i^\pi; T_i$	$J_f^\pi; T_f$	ΔE_C	$\Lambda\Sigma$	Δ	S_Λ	S_N	T	ΔE^{th}	ΔE^{exp}
$1/2_1^+; 0$	$3/2_1^+; 0$			0.735	-2.232	0.022	-8.921		
		0	44	213	33	-7	-200	83	<100
$1/2^+; 1$	$3/2_1^+; 0$			0.257	-0.756	0.015	-2.957		
		2313	-57	75	11	-5	-66	2268	2268
$1/2_2^+; 0$	$1/2^+; 1$			-0.899	-0.104	-1.363	0.122		
		1635	41	-261	2	446	3	1851	(1961)
$3/2_2^+; 0$	$1/2^+; 1$			0.471	0.028	-1.331	-0.239		
		1635	106	137	0	435	-5	2304	(2442)
$3/2_2^+; 0$	$1/2_2^+; 0$			1.365	0.136	0.032	-0.361		
		0	65	396	-2	-11	-8	453	(481)

while in jj coupling the states are 85% $p_{1/2}^{-2}$, 74% $p_{1/2}^{-1} p_{3/2}^{-1}$, and 93% $p_{1/2}^{-2}$, respectively. The Gamow-Teller matrix element is very closely related to the $\langle \sigma \tau \rangle$ matrix element for the core $0^+; 1 \to 1^+; 0 M1$ transition in ^{14}N, which is given by

$$\langle \sigma \tau \rangle \propto \sqrt{3} a(^1S) a(^3S) + a(^1P) a(^3P), \qquad (17)$$

with the amplitudes to be taken from Eq. (16).

The contributions to the energy spacings from a shell-model calculation using the parameters of Eq. (15) are given in Table III. Starting with the ground state, the energy shifts due to Λ-Σ coupling are calculated to be 59, 15, 116, 75, and 10 keV.

The coefficients that enter the ground-state doublet spacing show a significant shift away from the jj-coupling limit, in which the coefficients are $-3/2$ times those in Eq. (3). Specifically, the changes from 0.5 to 0.74 for Δ and from -12 to -9 for T mean that the higher spin member of the doublet is predicted to be the ground state in contrast to the usual ordering for p-shell hypernuclei, including $^{16}_{\Lambda}$O. This spacing was measured to be $E(1/2^+_1) - E(3/2^+_1) > -100$ keV, and thus the calculated spacing, 83 keV, is consistent with the data.

The excitation energy of the $1/2^+; 1$ state, which gets a significant contribution from Λ-Σ coupling, is well reproduced. Note that the contribution of S_N is small and would be zero in the jj limit of $p_{1/2}^{-2}$ for both core states. Viewed from another perspective, the coefficient of S_N for the $1/2^+; 1$ state depends strongly on the matrix element connecting the ^1S and ^3P components of the core wave function in Eq. (16). These components are sensitive to the p-shell interaction used. For example, the Cohen and Kurath interactions [47] give rise to amplitudes of ~ 0.53 for the ^3P component, a smaller coefficient of S_N in the hypernuclear calculation, and an energy for the $1/2^+; 1$ state that is higher by more than 100 keV.

The level spacings of the members of the excited-state doublet $(3/2^+_2, 1/2^+_2)$ from the $1/2^+; 1$ state and the doublet spacing itself are calculated to be 2304, 1851, and 453 keV, respectively. This upper-doublet spacing is dominantly given by Δ because the core state ^{14}N$(1^+; 0)$ is mainly ^3S in nature. This doublet spacing is not experimentally determined, but the observed 2442- and 1961-keV γ rays are likely to be the transitions from the upper-doublet members. Comparing the measured energy difference, 481 or -481 keV, with the calculated value, 453 keV, the assignments shown in the last column of Table III are strongly indicated. For this assumption, the doublet spacing is well reproduced using the parameter set in Eq. (15). On the other hand, the excitation energies of both members of the excited-state doublet are underestimated by about 100 keV. Here, S_N provides the dominant contribution to the shift of the centroid of the doublet above the unperturbed core energy separation of 3948 keV, and there is some dependence on the shell-model wave functions for the core. For example, the coefficient of S_N for the third and fourth entries in Table III would be -1.5 in the jj-coupling limit.

C. Electromagnetic transitions

The influence of the ΛN parameters on the spectra of $^{16}_{\Lambda}$O and $^{15}_{\Lambda}$N has been discussed in the preceding two subsections, and some use of the spectra and transition rates from the shell-model calculations has already been made in interpreting the results of this experiment in Sec. V. The electromagnetic lifetimes and branching ratios for the observed transitions are largely controlled by the $M1$ matrix elements for the three core transitions in ^{15}O and ^{14}N. For the upper doublets in both hypernuclei, the transition rates are governed by strong $M1$ transitions. Consequently, the lifetimes are short ($\sim$fs), and the deexcitation γ-ray lines are strongly Doppler broadened. For similar reasons, the γ-ray branching ratio for the 1^-_2 level of $^{16}_{\Lambda}$O differs little from the simple weak-coupling estimate (2:1 in favor of the 0^- final state).

The situation is very different for the decay of the $1/2^+; 1$ state of $^{15}_{\Lambda}$N because (1) the measured lifetime of $1.5 \pm 0.3 \pm 0.3$ ps is much longer than 0.1 ps for the core transition (Sec. V B5) and (2) the limit of 9% for the γ-ray branch to the $1/2^+$ member of the ground-state doublet is much less than 33% in the weak-coupling limit (Sec. V B7).

The $B(M1)$ values are given by

$$B(M1) = \frac{3}{4\pi} \frac{2J_f + 1}{2J_i + 1} M^2 \mu_N^2, \qquad (18)$$

where M is the reduced matrix element of the $M1$ operator. The $M1$ core transitions of interest, the magnetic moments of ^{14}N, ^{15}N, and ^{15}O, and many other $M1$ properties of p-shell nuclei are well described by the present wave functions together with an effective $M1$ operator [46] that specifies the six $M1$ matrix elements in the p shell (equivalently, the isoscalar and isovector g factors for the operators $\boldsymbol{l}$, $\boldsymbol{s}$, and $[Y^2, \boldsymbol{s}]^1$). For the $0^+; 1 \to 1^+_1; 0$ and $0^+; 1 \to 1^+_2; 0$ transitions in ^{14}N, the values of M are calculated to be -0.251 and 2.957, respectively [46]. The matrix elements contain similar negative orbital contributions, while the spin contributions are ~ 0 and large and positive, respectively, according to Eq. (17).

The corresponding matrix elements M for the $1/2^+; 1 \to 1/2^+; 0$ and $3/2^+; 0$ transitions in $^{15}_{\Lambda}$N are the same in the weak-coupling limit and equal to -0.251 [the 2:1 branching ratio comes from the $2J_f + 1$ factor in Eq. (18)]. The shell-model calculation admixes small $1^+_2 \times s_\Lambda$ components into the final-state wave functions with positive amplitudes of 0.050 and 0.032 for the $1/2^+$ and $3/2^+$ final states. This reduces the matrix element for the $1/2^+; 1 \to 1/2^+; 0$ transition from -0.25 to -0.10 and the $1/2^+; 1 \to 3/2^+; 0$ matrix element by a smaller amount. The net effect is to increase the lifetime of the $1/2^+; 1$ state by about a factor of 5 over the weak-coupling limit (to $\tau = 0.48$ ps) while the branch to the $1/2^+; 0$ state is reduced to 18%. These effects are in the right direction but not large enough to explain the experimental results.

With the present wave functions, the dominant contributions to the off-diagonal matrix elements between the $1^+_1; 0 \times s_\Lambda$ and $1^+_2; 0 \times s_\Lambda$ basis states are from S_N followed by contributions from T that are constructive for the $1/2^+$ state and destructive for the $3/2^+$ state [46]. The larger off-diagonal

matrix element for the $1/2^+$ case means that the γ-ray branch to the $1/2^+$ state is suppressed relative to the $3/2^+$ state (unless the mixing is large enough to change the sign of the $M1$ matrix element). If the amplitudes of the $1_2^+; 0 \times s_\Lambda$ admixtures are scaled up (by a factor of ~ 1.6) to reproduce the measured lifetime $\tau = 1.5 \pm 0.3 \pm 0.3$ ps, the γ-ray branch to the $1/2^+$ state drops to $\sim 3.5\%$, which is consistent with the limit derived in Sec. VB7. These results are sensitive to the choice of p-shell wave functions. It is also worth mentioning that the admixtures of Σ configurations contribute roughly $+0.01$ to the $M1$ matrix elements in either case [46] and that these are significant compared to the $M = -0.083$ for the $1/2^+; 1 \rightarrow 3/2^+$ transition that reproduces the measured lifetime.

D. Spin-dependent parameters from the present data

Tables II and III show that the parameter set in Eq. (15), which was derived to reproduce the $^{16}_{\Lambda}$O levels while using a fixed Λ-Σ coupling, also reproduces quite well the upper-doublet spacing and the $1/2^+; 1$ excitation energy in $^{15}_{\Lambda}$N, but it predicts a value for the excitation energy of the upper doublet in $^{15}_{\Lambda}$N that is somewhat too small. The Λ-spin-orbit parameter S_Λ is fixed to be small by the γ-ray data for $^9_{\Lambda}$Be [2,3]. The theoretical breakdown of the contributions to the measured energy spacings in Tables II and III then shows that Δ, S_N, and T are well determined, because Δ and S_N dominate in certain spacings while the ground-state doublet spacings involve a delicate cancellation between significant contributions from both Δ and T. It is this cancellation that fixes T to be small and positive based on the measured spacing of the ground-state doublet in $^{16}_{\Lambda}$O, in general agreement with the predictions of YN models, $T = 0.01$–0.06 MeV, as described in Sec. IC.

The matrix elements Δ and S_N take values that are somewhat smaller than the corresponding quantities in Eq. (2) that are determined primarily from $^7_{\Lambda}$Li. This is what would be expected if the nuclei at the end of the p shell were significantly larger than those at the beginning of the shell. However, it is well known that the charge radii of stable p-shell nuclei are almost constant throughout the shell [48,49], essentially because the p-shell nucleons become more deeply bound for the heavier nuclei. In fact, if one calculates the ΛN matrix elements from a YNG interaction using Woods-Saxon wave functions, they tend to be slightly larger for $A = 16$ than for $A = 7$ [50]. This is what led to the choice of $\Delta = 0.468$ MeV in the first analysis of our $^{16}_{\Lambda}$O data [29]. Now, the data on the upper doublets in $^{16}_{\Lambda}$O and $^{15}_{\Lambda}$N (with some reservations) imply a smaller value of $\Delta = 0.290$ MeV.

Confidence in this value of Δ is increased by the fact that the ground-state doublet spacing in $^{11}_{\Lambda}$B has been established as 264 keV [28,51,52] and is reproduced by this value of Δ [46]. It is notable that a value $\Delta < 0.30$ MeV was proposed [53] to account for the nonobservation of the ground-state doublet transition in $^{10}_{\Lambda}$B above 100 keV in the first hypernuclear experiment with Ge γ-ray detectors [54] (a result confirmed in the present experiment using a ^{10}B target [28]).

VII. SUMMARY

A γ-ray spectroscopy experiment on $^{16}_{\Lambda}$O and $^{15}_{\Lambda}$N was performed at the BNL AGS D6 beamline employing a high-quality 0.93 GeV/c K^- beam and the Hyperball Ge detector array. The experiment is one of a series aimed at studies of spin-dependent ΛN interactions through the precise measurement of γ-ray transitions in p-shell hypernuclei. The bound states of both hypernuclei were produced via the ^{16}O(K^-, π^-) reaction. We succeeded in observing three γ-ray transitions in $^{16}_{\Lambda}$O and three in $^{15}_{\Lambda}$N.

For $^{16}_{\Lambda}$O, we determined the level scheme for the four bound negative-parity states [two doublets, $(1_1^-, 0^-)$ and $(2^-, 1_2^-)$] from these γ rays, although another assignment for the 2^- state is not excluded. In particular, we determined the excitation energy of the 1_2^- state to be $6561.7 \pm 1.1 \pm 1.7$ keV and found a small spacing of $26.4 \pm 1.6 \pm 0.5$ keV for the ground-state doublet $(1^-, 0^-)$ with the 0^- state being the ground state. The doublet spacing determines a small but nonzero strength for the ΛN tensor interaction, and this is the first experiment to give direct information on the ΛN tensor interaction. One of the three γ rays in $^{16}_{\Lambda}$O is likely to be a transition from the 2^- spin-flip state to the one of the ground-state doublet members $(2^- \rightarrow 1_1^-)$, and this constitutes the first observation of the direct production of a spin-flip state via the (K^-, π^-) reaction.

For $^{15}_{\Lambda}$N, we observed a rather sharp 2268-keV γ ray and measured the corresponding lifetime via the Doppler-shift attenuation method to be 1.5 ± 0.4 ps. The γ ray was interpreted as a transition from the $1/2^+; 1$ level of $^{15}_{\Lambda}$N to the $3/2^+; 0$ member of the ground-state doublet. Because the transition to the $1/2_1^+; 0$ member of the ground-state doublet was not observed (a limit of $<9\%$ was put on the γ-ray branch), the spacing and the spin ordering of the ground-state doublet were not determined, but we obtained an upper limit on the spacing energy of $E(1/2_1^+) - E(3/2_1^+) > -100$ keV. We also observed the γ-ray transitions which can be assigned to those from the upper-doublet states $(3/2_2^+, 1/2_2^+)$ to the $1/2^+; 1$ state.

We also measured the reaction angle $(\theta_{K\pi})$ distributions of the $^{16}_{\Lambda}$O and $^{15}_{\Lambda}$N γ rays. Analysis of the distributions of $^{15}_{\Lambda}$N γ rays provides information on the spins of the initial states of $^{16}_{\Lambda}$O decaying to the excited states of $^{15}_{\Lambda}$N via proton emission.

The level spectra obtained for $^{15}_{\Lambda}$N and $^{16}_{\Lambda}$O are consistently explained by the set of values for the ΛN interaction parameters Δ, S_N, and T in Eq. (15). The determination of T was, in fact, the main motivation for the present experiment.

[1] H. Tamura *et al.*, Phys. Rev. Lett. **84**, 5963 (2000).

[2] H. Akikawa *et al.*, Phys. Rev. Lett. **88**, 082501 (2002).

[3] H. Tamura *et al.*, Nucl. Phys. **A754**, 58c (2005).

[4] Th. A. Rijken, V. G. J. Stoks, and Y. Yamamoto, Phys. Rev. C **59**, 21 (1999) and references therein.

[5] Th. A. Rijken and Y. Yamamoto, Phys. Rev. C **73**, 044008 (2006).

[6] Y. Yamamoto, T. Motoba, H. Himeno, K. Ikeda, and S. Nagata, Prog. Theor. Phys. Suppl. **117**, 361 (1994).

[7] T. T. S. Kuo and J. Hao, Prog. Theor. Phys. Suppl. **117**, 351 (1994).

[8] Y. Tzeng, S. Y. Tsay Tzeng, T. T. S. Kuo, and T.-S. H. Lee, Phys. Rev. C **60**, 044305 (1999).

[9] Y. Akaishi, T. Harada, S. Shinmura, and K. S. Myint, Phys. Rev. Lett. **84**, 3539 (2000).

[10] E. Hiyama, M. Kamimura, T. Motoba, T. Yamada, and Y. Yamamoto, Phys. Rev. C **65**, 011301(R) (2001).

[11] A. Nogga, H. Kamada, and W. Glöckle, Phys. Rev. Lett. **88**, 172501 (2002).

[12] H. Nemura, Y. Akaishi, and Y. Suzuki, Phys. Rev. Lett. **89**, 142504 (2002).

[13] A. Gal, J. M. Soper, and R. H. Dalitz, Ann. Phys. (NY) **63**, 53 (1971).

[14] D. J. Millener, A. Gal, C. B. Dover, and R. H. Dalitz, Phys. Rev. C **31**, 499 (1985).

[15] D. J. Millener, Nucl. Phys. **A754**, 48c (2005).

[16] H. Tamura, Nucl. Phys. **A639**, 83c (1998).

[17] M. Bedjidian *et al.*, Phys. Lett. **B83**, 252 (1979).

[18] B. F. Gibson and D. R. Lehman, Phys. Rev. C **37**, 679 (1988).

[19] W. Brückner *et al.*, Phys. Lett. **B79**, 157 (1978).

[20] A. Bouyssy, Phys. Lett. **B84**, 41 (1979).

[21] M. May *et al.*, Phys. Rev. Lett. **51**, 2085 (1983).

[22] S. Ajimura *et al.*, Phys. Rev. Lett. **86**, 4255 (2001); H. Kohri *et al.*, Phys. Rev. C **65**, 034607 (2002).

[23] D. J. Millener, in *Hypernuclear Physics with Electromagnetic Probes*, edited by L. Tang and O. Hashimoto (Hampton University, Hampton, VA, 1999), p. 79.

[24] M. Ukai *et al.*, Phys. Rev. C **73**, 012501(R) (2006).

[25] E. H. Auerbach, A. J. Baltz, C. B. Dover, A. Gal, S. H. Kahana, L. Ludeking, and D. J. Millener, Ann. Phys. (NY) **148**, 381 (1983).

[26] D. H. Davis and D. N. Tovee (unpublished, private communication).

[27] O. Hashimoto *et al.*, Nucl. Phys. **A639**, 93c (1998).

[28] O. Hashimoto and H. Tamura, Prog. Part. Nucl. Phys. **57**, 564 (2006).

[29] M. Ukai *et al.*, Phys. Rev. Lett. **93**, 232501 (2004).

[30] M. Juric *et al.*, Nucl. Phys. **B52**, 1 (1973); T. Cantwell *et al.*, Nucl. Phys. **A236**, 445 (1974); P. Dluzewski, K. Garbowska-Pniewska, J. Pniewski, T. Tymieniecka, P. Ciok, and D. H. Davis, Nucl. Phys. **A484**, 520 (1988).

[31] A. Gal, Phys. Rev. C **28**, 2186 (1983).

[32] L. Majling, R. A. Eramzhyan, and V. N. Fetisov, Czech. J. Phys. **42**, 1197 (1992).

[33] P. H. Pile *et al.*, Nucl. Instrum. Methods A **321**, 48 (1992).

[34] Supplied by EG&G ORTEC, Advanced Measurement Technology, Inc., 801 South Illinois Avenue, Oak Ridge, TN 37831-0895, USA.

[35] Universal Memory Module, http://km.phys.sci.osaka-u.ac.jp/ajimura/mem/

[36] H. Tamura *et al.*, Prog. Theor. Phys. Suppl. **117**, 1 (1994).

[37] J. F. Ziegler *et al.*, The Stopping and Range of Ions in Matter, available at the URL http://www.srim.org.

[38] R. H. Dalitz and A. Gal, Ann. Phys. (NY) **116**, 167 (1978).

[39] K. Tanida *et al.*, Phys. Rev. Lett. **86**, 1982 (2001).

[40] H. Hotchi *et al.*, Phys. Rev. C **64**, 044302 (2001).

[41] F. Ajzenberg-Selove, Nucl. Phys. **A523**, 1 (1991).

[42] W.-M. Yao *et al.*, J. Phys. G **33**, 1 (2006).

[43] S. Kameoka *et al.*, Nucl. Phys. A **754**, 173c (2005).

[44] R. Grace *et al.*, Phys. Rev. Lett. **55**, 1055 (1985).

[45] H. Bhang *et al.*, Phys. Rev. Lett. **81**, 4321 (1998).

[46] D. J. Millener, in *Topics in Strangeness Nuclear Physics,* Lecture Notes in Physics, Vol. 724, edited by P. Bydzovsky, A. Gal, and J. Mares (Springer, New York, 2007), p. 31.

[47] S. Cohen and D. Kurath, Nucl. Phys. **73**, 1 (1965).

[48] D. H. Wilkinson and M. E. Mafethe, Nucl. Phys. **85**, 97 (1966).

[49] H. de Vries, C. W. de Jager, and C. de Vries, At. Data Nucl. Data Tables **36**, 495 (1987).

[50] D. J. Millener, Nucl. Phys. **A691**, 93c (2001).

[51] Y. Miura *et al.*, Nucl. Phys. **A754**, 75c (2005).

[52] Y. Ma *et al.*, Eur. Phys. J. A **33**, 243 (2007).

[53] V. N. Fetisov, L. Majling, Žofka, and R. A. Eramzhyan, Z. Phys. A **339**, 399 (1991).

[54] R. E. Chrien *et al.*, Phys. Rev. C **41**, 1062 (1990).